# NUMERICAL MODELLING OF MEDIUM SCALE INDENTATION TESTS



BIN LIU

# Numerical Modelling of Medium Scale Indentation Tests

by

© Bin Liu, B.Eng.

A thesis submitted to the School of Graduate Studies
in partial fulfillment of the requirements for the degree of
Master of Engineering

Faculty of Engineering and Applied Science
Memorial University of Newfoundland
Janurary, 1994

ISBN 0-315-96083-3

Canada

## Abstract

Medium scale indentation tests were conducted at Hobson's Choice Ice Island in 1989 and 1990. Areas with different degrees of damage were found in the ice close to the indentor in these tests. It is believed that the fluctuation of the total ice load and local peak pressure is determined by the dynamic behaviour of the ice at the hard spots or the 'critical zones'. The high confinement pressure at hot spots may have a great effect on the failure process. A review of the mechanical properties of ice and the damage theory is given. The effects of hydrostatic pressure on ice deformation and damage development are discussed. One of the tests from the Hobson's Choice Ice Island experiments is modelled using the finite element method.

Damage theory and the effects of hydrostatic pressure are considered in the theoretical modelling of the indentation process. The results of the numerical modelling are compared with the results of the test and good agreement has been found. Further investigation on the effects of hydrostatic pressure is suggested.

# Acknowledgements

I greatly appreciate the academic guidance and financial support from my supervisor, Dr. Ian Jordaan whose thoughtful suggestions, constructive comments and detailed instruction upon every aspect at every stage made it possible for me to complete this research. Special thanks are given to Mr. Jing Xiao and Mr. Mark Fuglem for their great help and valuable suggestions. Thanks to Dr. J. Molgaard for his instruction and introduction of important knowledge to me. Finally, I wish to thank my colleagues, Bin Zou, Sanjay Sing, Peter Brown, Michelle Johnston, Barry Stone and Shawn Kenny for their sincere concerns and help.

# Contents

# List of Figures

# Nomenclature

| | |
|---|---|
| $\sigma_{ij}$ | stress tensor (MPa) |
| $\epsilon_{ij}$ | strain tensor |
| $E$ | elastic modulus (MPa) |
| $E_k$ | elastic stiffness in Kelvin unit |
| $E_m$ | elastic stiffness in Maxwell unit |
| $G$ | shear modulus (MPa) |
| $K$ | bulk modulus (MPa) |
| $\nu$ | Poisson's ratio |
| $t$ | time (s) |
| $\mu$ | viscosity coefficient (MPa·s) |
| $\mu_k$ | viscosity in Kelvin unit |
| $\mu_m$ | viscosity in Maxwell unit |
| $C_{ijkl}$ | fourth order compliance tensor |
| $\epsilon_{ij}^e$ | elastic strain components |
| $\epsilon_{ij}^d$ | delayed elastic strain components |
| $\epsilon_{ij}^c$ | secondary creep strain components |
| $e_{ij}^e$ | elastic strain deviator |
| $e_{ij}^d$ | delayed elastic strain deviator |
| $e_{ij}^c$ | secondary creep strain deviator |
| $e$ | equivalent strain |
| $\epsilon_v$ | volumetric strain |
| $\sigma_v$ | volumetric stress (MPa) |
| $s$ | von Mises stress (MPa) |
| $s_{ij}$ | stress deviator (MPa) |
| $\sigma_c$ | critical stress for crack nucleation (MPa) |
| $d$ | average grain size (m) |
| $a$ | one half of the crack length (m) |
| $N$ | crack density |

| | |
|---|---|
| $D_N$ | damage measurement based on crack density |
| $\dot{N}_0$ | initial crack density rate |
| $\beta$ | creep enhancement parameter |
| $\dot{\epsilon}_0^d$ | delayed elastic strain reference rate |
| $\dot{\epsilon}_0^c$ | secondary creep strain reference rate |
| $\delta_{ij}$ | delta function |
| $m$ | damage exponent for damage measurement $D_N$ |
| $n$ | creep exponent |
| $S_\epsilon$ | damage parameter |
| $q$ | damage exponent |
| $S_0$ | damage constant |
| $F(p)$ | pressure hardening factor |
| $G(p)$ | pressure softening factor |
| $F_0$ | pressure hardening constant |
| $G_0$ | pressure softening constant |
| $M$ | pressure softening parameter |
| $f$ | pressure hardening exponent |
| $g$ | pressure softening exponent |
| $p_0$ | reference pressure |

# Chapter 1

# Introduction

Exploration for offshore natural resources, such as oil, gas, mineral deposits and hydrocarbon reserves has been taking place since the early 1970's. Most of these resources in Canada are situated on the continental margins. Exploration and recovery of these resources are challenged by the severe environmental conditions. In addition to the usual hazards in conventional environments such as waves and ship collisions, offshore structures in Arctic and sub-Arctic waters must cope with ice loading. It is recognized that the interaction of ice with marine structures is a major design consideration. Difficulties in ice force estimation arise because of the unique structure and behaviour of ice as well as the near-melting temperatures in which it operates.

Ice in nature is a polycrystalline material with a large number of single crystals in different orientations. This polycrystalline material could be classified into two kinds: granular ice and columnar ice. Columnar ice is formed with the grains growing parallel to the heat flow and with c-axis perpendicular to the column length. This type of ice is referred to as S2 ice and can be found in lakes, rivers and seas. Its mechanical properties are orthotropic. In granular ice, the grains are

randomly oriented. The size of the grain is found to range from fine to medium. This type of ice can be found in icebergs, lakes and seas and can be treated as a statistically isotropic material. Granular ice can be made in the laboratory by freezing water seeded with randomly oriented fine ice crystals. Ice behaves in a viscoelastic manner with its deformation dependent on the loading rate. When ice is stressed it exhibits an instantaneous elastic deformation and immediately begins to creep. The Burgers model which consists of a Kelvin unit and a Maxwell unit is used to characterize the mechanical properties of polycrystalline ice. According to Sanderson (1988), there are two typical aspects of ice behaviour: continuum and fracture. Continuum behaviour includes elastic, ductile creep deformation and damage process characterized by uniformly distributed microcracking.

Hazardous ice features are classified as level first year ice sheet, deformed first year ice features, multi-year ice floes and glacial ice features (icebergs and ice islands). Considering these ice conditions, an offshore structure may be loaded by discrete masses such as multi-year floes or icebergs, a continuous first-year ice cover and a large ice feature surrounded by first-year ice. Ice features mentioned above are set in motion under the effect of environmental forces.

When a marine structure obstructs this motion, the interaction between the ice feature and the structure may end immediately if the forces exerted by the structure introduce sufficient inertial forces to stop the ice feature or change its direction of motion. In this case there would not be any contact any more. If the driving force is high enough, the structure will be fully enveloped in the ice feature soon after the interaction starts. The width of the structure is the contact width and local indentation occurs continuously during the interaction. In most cases, the ice cover

is large enough so that its movement will not be affected by the structure and the structure is fully embedded in the ice. The force can be calculated from the local stresses of the ice along the width of the structure. The total ice force is the sum of local stresses.

The interaction between a vertical structure and an ice sheet is a very common ice-load scenario. Because of the confinement effect of the ice in the area of load application, a triaxial state of stress develops in the ice behind the indentor. If the failure due to global fracture does not occur, the total ice force can be obtained by analyzing the stresses in indentation. An appropriate model of the whole interaction system including ice feature and structure and a good understanding of the constitutive behaviour and size effects of ice are necessary to obtain an accurate estimate of ice force.

The average global ice pressures recorded in small-scale laboratory indentation tests, medium scale indentation tests and full scale impacts of multi-year sea ice with artificial islands range from 10 MPa to 0.5 MPa and lower. The bigger the scale of interaction, the smaller the average global pressure. This variation between measured index mechanical properties and full-scale ice behaviour is known as the scale effect. This phenomenon is generally associated with non-simultaneous failure and the statistical distribution of zones of high pressure in the contact area. The ice structure interaction is further complicated by the various modes of failure of the ice adjacent to the structure. Although the crushing mode is generally observed during interaction events, the process can be compounded by mixed-mode deformation, such as crushing coupled with splitting, out of plane flexure, spalling, or buckling. Moreover, the interaction events depend on many factors. The factors

commonly involved are the loading rate (the speed of the ice sheet), temperature, mechanical properties of ice and structure, degree of confinement and the shape of the interface. The results of recent field and laboratory investigations indicate that pressure melting and sintering are also active mechanisms.

The appearance of dynamic ice-structure interaction was thought to be most pronounced in slender, flexible, bottom-founded structures with small, internal damping such as lighthouses and small platforms. In the winter of 1986, however, the Beaufort Sea structure Molikpaq experienced severe vibrations caused by the repeated crushing failure of a multi-year ice floe which produced an eight meter high pile of pulverized ice adjacent to the structure (Jefferies and Wright, 1988).

Since structural analysis is quite advanced, a good theoretical model for an offshore structure is not difficult to establish. To simplify the analysis, it is only necessary to consider those modes of structural vibration that will be excited during the interaction. Sometimes it is sufficient to model the structure for its fundamental mode of vibration by a single-degree-of-freedom system with a mass M attached to a spring of stiffness K and linear damping element of coefficient C. The differential equation governing its motion is:

$$M\ddot{x} + C\dot{x} + Kx = F(t) \tag{1.1}$$

where $x$ is the displacement, $\dot{x}$ the velocity, $\ddot{x}$ the acceleration of the mass and $F(t)$ the interaction force generated between the ice sheet and the structure. Equations similar to this can be derived for a multi-degree-freedom system through modal analysis for each of the different modes of vibration. The condition of stability for a structure can be found by solving the roots of the above equation.

A variety of mathematical models have been developed for describing the ice-induced vibration. Most of them treat the structure as a spring-mass-damper element, but they differ in how the interaction forces F(t) are assumed or treated. The interaction between a moving ice sheet and a fixed structure results in loading and deformation of both the structure and the ice sheet. Any theoretical treatment must stress the interaction aspect of this problem.

Jefferies and Wright presented a conceptual framework for dynamic ice-structure interaction during crushing events in the following steps:

1. The ice approaches the structure.
2. The structure deflects.
3. The ice crushes at its failure stress.
4. Due to the ice failure, there is a spring-back of both the structure and the ice. The stored elastic energy is released and the the crushed ice is extruded out of the zone in front of the structure.
5. The process repeats.

Through the analysis of this process, the action of several parameters has been identified:

1. The peak load is the fracture strength of the ice.
2. The minimum load is controlled by the crushed ice extrusion mechanism.
3. The frequency is controlled by a combination of the ice velocity, the combined ice-structure stiffness and the difference in the peak and the minimum ice load.

4. The unloading rate will be controlled by the inertial effects and the extrusion mechanism.

It is believed that micro-cracking plays an important role in transforming an intact ice sheet into a heap of granular particles as observed in ice crushing. Cracking activity in the vicinity of the indenter leads to failure of ice, resulting in sudden unloading. In this case, the frequency of the fluctuation in the ice forces can be related to the velocity and the length of the damage zone in the ice.

The most significant crushing processes are pulverization and clearing (Jordaan, 1988). In the initial stages of pulverization, sets of micro-cracks emerge and they are distributed in certain patterns. The stain energy accumulates gradually in the ice. This energy will be rapidly released when a large enough number of micro-cracks appear, accompanied by an abrupt drop in the indentation force. The strain energy is dissipated in the damage process, i.e., by the transformation from strain energy into other kinds of energy through friction between ice particles moving very quickly relative to each other.

The extrusion of pulverized ice was treated as a viscous flow by Jordaan and Timco (1988) and a stick-slip movement model was proposed by Jordaan and McKenna (1991). Based on the energy dissipation analysis, a dynamic equilibrium equation might be established. At present, a precise calculation of each term of energy is still impossible. There is still a need to conduct careful laboratory tests to investigate the ice-structure interaction.

Numerical methods have been used to solve indentation problems related to the damage process in ice. It is considered that the finite element method is a promising approach in modeling ice and structure behaviour. Despite the accelerating growth

of literature on the subject of ice forces on structures in the last two decades, the available models are not yet fully satisfactory. Practical design problems have been dealt with by concentrating on empirical results and conservative idealizations. The focus of this thesis is to investigate the ice behaviour in crushing. Some new approaches about failure mechanisms involved are developed. The scope of this work includes the following tasks:

1. a literature review of the mechanical properties of ice,
2. an analysis and discussion of the volumetric stress effect on ice deformation and failure in indentation,
3. a description of small scale laboratory tests and medium scale indentation tests,
4. numerical modelling of a medium scale indentation test and comparison of the modelling results with the experiment results, and
5. conclusions and recommendations for future work.

The most important work is the numerical modelling of the medium scale indentation tests conducted at Hobson's Choice Ice Island in 1990. In this modelling, some new ideas on the constitution of ice are applied through the finite element method.

# Chapter 2

# Ice Mechanical Properties

## 2.1 Viscoelastic Model

The behaviour of viscoelastic materials is modeled by using combinations of two basic elements: spring and dashpot. A four-element rheological model for polycrystalline ice, i.e. Burgers model, was therefore presented by Jordaan et al. (1988). Parameters are calibrated from the results of small uniaxial ice tests. Through the process of the calibration, this model can describe the behaviour of ice very well. Satisfactory results are also obtained by finite element simulation of indentation tests using Burgers model.

### 2.1.1 Elasticity of Ice

Granular ice, treated as an isotropic material in engineering problems, is characterized by two constants in its elastic behaviour: the elastic modulus E, and the Poisson's ratio, $\nu$. The elastic strain of ice is represented by Hooke's law as for other materials:

$$\epsilon = \sigma / E. \tag{2.1}$$

To obtain the elastic modulus and Poisson's ratio, one must take care in estimating the time-dependent effect in the ice stress test. A true estimate can only be obtained from a very rapid test. In static tests, the elastic modulus is determined by reading the initial tangent value from a stress-strain curve. This proves to be not very accurate since ice creeps at any stress. Dynamic methods are therefore employed which can minimize the time-dependent effect.

The variation of elastic modulus and Poisson's ratio with temperature, as given by Sinha (1989a) for both granular and columnar ice, shows that temperature does not have a strong effect. The elastic modulus and Poisson's ratio are 9 GPa and 0.308 at temperature of $-50°C$, and 10.6 GPa and 0.3605 at temperature of $0°C$. The elastic modulus is not highly dependent on grain size either (Sanderson 1988). On the other hand, porosity has strong influence on the ice elastic properties. Measured values for the elastic modulus of sea ice are highly scattered ranging from 0.3 to 10 GPa for static tests and 6 to 10 GPa for dynamic tests. The scatter is due to the presence of impurities in the sea ice. Theoretical and experimental models for calculating the elastic modulus of sea ice as a function of brine volume have been proposed.

Considering the present field of interest, for polycrystalline ice of low porosity, the elastic modulus given by high frequency dynamic tests is about 9 to 9.5 GPa in the temperature from $-5°C$ to $-10°C$ (Mellor, 1983). The standard range of Poisson's ratio is 0.3 to 0.33.

### 2.1.2 Creep of Ice

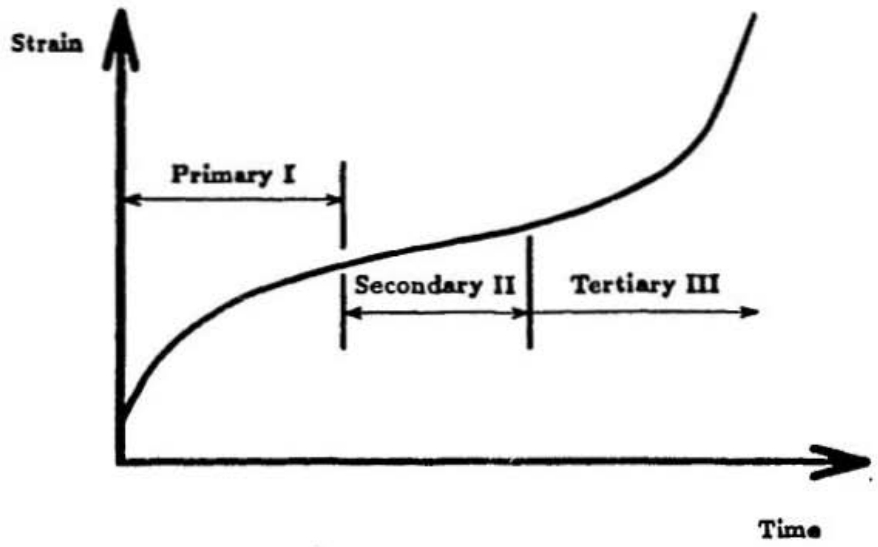


Figure 2.1: Three Stages of Ice Creep

A typical creep curve is shown in Figure 2.1. There are three distinct regions in this curve. First there is an initial transient creep which is also known as a primary creep. The primary creep is followed by a secondary steady-state phase and this secondary creep is also called minimum creep because in all three phases, the second creep rate is the smallest. Finally, there is a tertiary creep and the creep rate increases again.

Delayed elastic (transient or primary creep) creep is similar to elastic deformation in that it is totally recoverable. Delayed elastic strain is associated with grain distortion and sliding due to the shear stresses generated between grain boundaries. Sinha (1978) gave an expression for delayed elastic strain under constant stress:

$$\epsilon^d(t) = \frac{c_1 d_1}{d}(\sigma/E)^s[1 - exp(-(\alpha_T t)^b)], \tag{2.2}$$

where $c_1, s, b$ and $\alpha_T$ are constants depending on the temperature and grain size d.

The secondary creep strain characterizes viscous flow, corresponding to dislocation movement within the grains, mostly slip in basal planes. The fact that basal slip is much easier than slip on other planes make the stress distribution in a loaded polycrystal become non-uniform as the loading starts. In randomly oriented granular ice, those grains that are the best oriented for basal shear will slip first and therefore the stress will become concentrated on those less well oriented. On the other hand, the most poorly oriented crystals tend to rotate in order to turn to an easier glide direction.

In the model of Sinha (1982), unlike the delayed elastic creep, the secondary creep rate is independent of grain size. There is still some debate as to whether the secondary or minimum creep is a fundamental material property or merely marks the transition from the primary to tertiary stages. Under certain conditions, the ice deformation will jump from primary to tertiary creep directly. Basically, this secondary creep is a non-recoverable deformation as a result of intragranular dislocation movements.

Glen's Law (Glen, 1955), also known as Norton's Law or simply the creep power law is the commonly accepted form of the constitutive equation for secondary creep rate for ice, i.e.

$$\dot{\epsilon} = A\sigma^n, \tag{2.3}$$

where n is a constant and A is a function of temperature in the form of:

$$A = Bexp(-Q/RT), \tag{2.4}$$

where $R = 8.314J\ mol^{-1}K^{-1}$, is the universal gas constant; $T$ is the temperature in degrees Kelvin; Q is the activation energy and B is a material constant. Neither

B nor Q is dependent on the ice type. In Sinha's equation for columnar ice, Glen's Law takes the form of:

$$\dot{\epsilon}^c = \dot{\epsilon}_0^c(\sigma/\sigma_0)^n, \tag{2.5}$$

where $\dot{\epsilon}_0, \sigma_0$ and $n$ are all creep constants. In multiaxial stress states, this equation can be written as:

$$\dot{\epsilon}_{ij}^c = 3\dot{\epsilon}_0^c/2(s/\sigma_0)^n s_{ij}/s, \tag{2.6}$$

where $s$ is the von Mises stress and $\dot{\epsilon}_{ij}$ and $s_{ij}$ are the strain and stress tensors respectively.

The tertiary creep is often associated with microcracking and the very large strain which may be the result of possible failure. It is also found that for tertiary creep to occur, microcracking does not necessary need to exist. According to Sanderson (1988), tertiary creep could be also initiated by dynamic recrystallization. Jordaan and McKenna (1989) point out that acceleration of creep rate could result from an increasing number of dislocation sites. Whether this acceleration in creep is due to damage such as microcracking or intrinsic response, or both of them is still unknown. As a matter of fact, the real tertiary process is not well understood. In this study, the tertiary creep effect is included in the secondary creep by considering the enhancement of creep due to cracks, recrystallization and pressure softening effects.

### 2.1.3 Constitutive Models

The time dependent deformational behaviour of linear viscoelastic solid under a uniaxial stress state can be expressed as:

$$\epsilon(t) = \int_0^t D(x, t - t') \frac{\partial \sigma(x, t')}{\partial t'} dt' \tag{2.7}$$

and

$$\sigma(t) = \int_0^t E(x, t - t') \frac{\partial \epsilon(x, t')}{\partial t'} dt', \tag{2.8}$$

in which $t'$ is a point of time in the interval $[0, t]$, D(.) and E(.) are creep (compliance) and relaxation (modulus) functions. The symbol $x$ is used to denote position in the material. Aging could be included by making D and E functions of time $t'$ in addition to the duration $(t - t')$ (Jordaan, 1990).

The compliance and modulus functions are related in the following way:

$$P^2 \bar{D}(x, P) \bar{E}(x, P) = 1, \tag{2.9}$$

where the bar indicates the Laplace transform and P is the parameter of the transform. Based on the thermodynamics of irreversible processes, the creep compliance and relaxation modulus are expressed in following:

$$D(x, t') = \frac{1}{E_1(x)} + \frac{t - t'}{\eta_1(x)} + \sum_{i=2}^{N} \frac{1}{E_i(x)} \{1 - exp[-\frac{E_i(x)}{\eta_i(x)}(t - t')]\} \tag{2.10}$$

and

$$E(x, t - t') = E_1(x) + \sum_{i=2}^{N} E_i(x) exp[-\frac{\eta_i'(x)}{E_i'(x)}]. \tag{2.11}$$

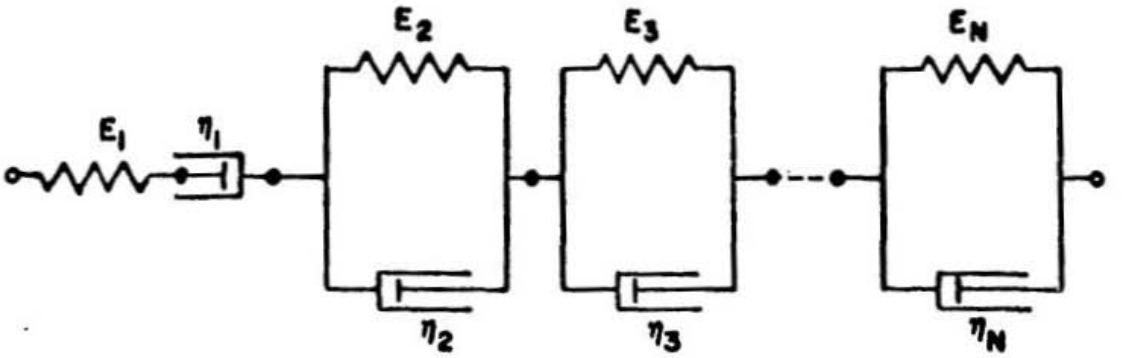


Figure 2.2: Kelvin Chain

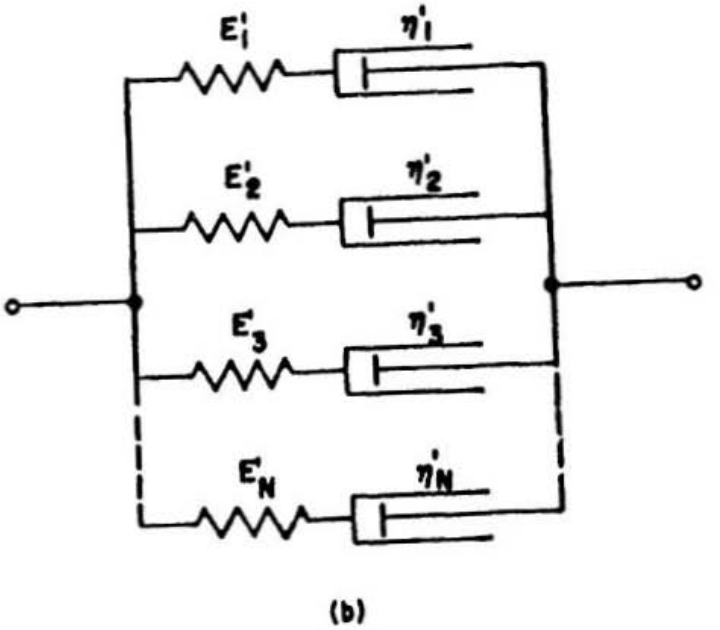


Figure 2.3: Maxwell Chain

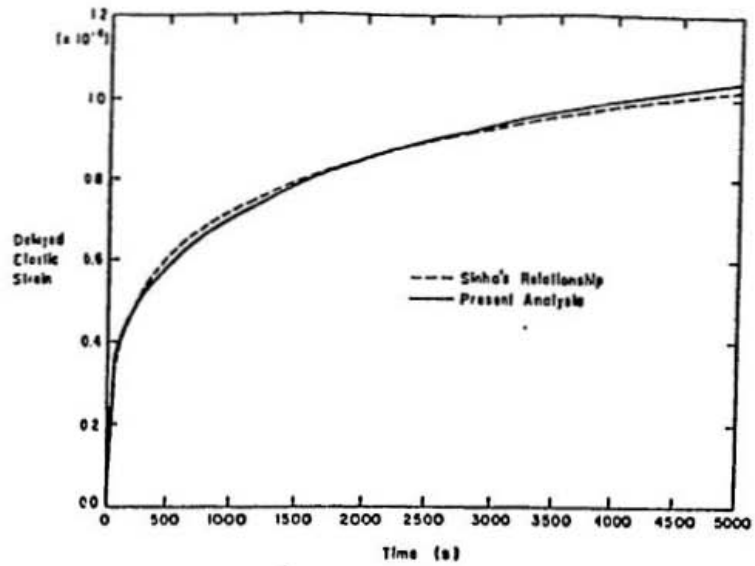


Figure 2.4: The Strain-Time Curves of Sinha's Equation and the Model of Two Kelvin Units (Jordaan et al., 1988)

Figure 2.2 and Figure 2.3 show series of springs and dashpot which represent the viscoelastic material described by above equations. The summation term in the creep compliance equation is the delayed elastic creep which is represented by Figure 2.3. The values of $E, E', \eta, \eta'$ can be interpreted as stiffness (moduli) and dashpot viscosity.

The above creep compliance function is convenient in solving simple stress state problems. For instance, it can be used to obtain strain response of ice under non-uniform stress condition, i.e. $\partial\sigma(x,t')/\partial t' = constant$. All parameters in the solution can be derived by fitting the solution to the test data using a optimization method. As an example, the delayed elastic strain caused by a stress with a constant stress rate calculated by using two Kelvin units in a series is presented in Figure 2.4 (Jordaan et al., 1988). For comparison, results from Sinha's equation under

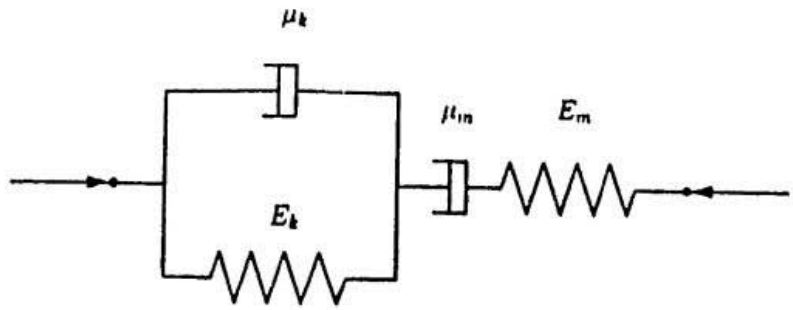


Figure 2.5: Burgers Model

same stress condition is also shown in the same Figure.

If the number $N$ in both summation terms of the above two equations is chosen to be 3, the creep compliance equation represents a linear Burgers model which will be discussed in detail later.

Jordaan et al. (1990) point out that for the series of Kelvin units a spectrum of retardation times with a distribution function is required. Due to the difficulties encountered in practice, one has to resort to a simpler model and hence a four element Burgers body is presented.

Before dealing with Burgers model, it is helpful to present Sinha's model first because of the close resemblance between the two models. As discussed in last section, it is generally accepted that ice deformation can be expressed as:

$$\epsilon_t = \epsilon_e + \epsilon_d + \epsilon_v, \tag{2.12}$$

where $\epsilon_t$ is the total strain, $\epsilon_e$ is the elastic strain, $\epsilon_d$ is the delayed elastic deformation and $\epsilon_v$ is the secondary creep. Sinha formulates the total strain as:

$$\epsilon_t = \frac{\sigma}{E_0} + \frac{c_1 d_1}{d}(\sigma/E)^s[1 - exp(-(\alpha_T t)^b)] + \dot{\epsilon}_0^c(\frac{\sigma}{\sigma_0})^n t. \tag{2.13}$$

From Figure 2.5, it is seen that the Burgers model basically has two components: a Maxwell and a Kelvin unit. The Maxwell unit corresponds to the elastic and permanent creep in Sinha's equation. Following Flugge (1967), for uniform stress, the elastic strain and creep in the Maxwell unit are:

$$\epsilon_m = \frac{\sigma}{\mu(\sigma)}t + \frac{\sigma}{E_0}, \tag{2.14}$$

where $\sigma$ is the applied axial stress and $\mu(\sigma)$ is the stress dependent creep coefficient (viscosity). The delayed elastic strain is formulated by the Kelvin unit. If the stress on the spring of the Kelvin unit is $\sigma_s$ and the stress on the dashpot is $\sigma_d$, the applied axial stress is:

$$\sigma = \sigma_s + \sigma_d, \tag{2.15}$$

where:

$$\sigma_s = E_k\epsilon$$

and

$$\sigma_d = \mu_k(\sigma_d)\dot{\epsilon}. \tag{2.16}$$

By substituting, the applied axial stress:

$$\sigma = E_k\epsilon + \mu_k(\sigma_d)\dot{\epsilon}. \tag{2.17}$$

If $\sigma$ is a uniform stress then,

$$\frac{\mu_k(\sigma_d)}{E_k}\frac{\partial}{\partial t}(\sigma - E_k\epsilon) + (\sigma - E_k\epsilon) = 0. \tag{2.18}$$

With manipulation, this equation yields the final solution of delayed elastic strain:

$$\epsilon = \frac{\sigma}{E_K}[1 - exp(-\int_0^t \frac{E_K}{\mu_k(\sigma_d)}d\tau)], \tag{2.19}$$

where $E_K$ is the spring constant for the Kelvin unit and $\tau$ is an intermediate time. This solution is actually identical to Sinha's equation of delayed elastic strain except that the argument of the exponent is $-\int_0^t \frac{E_K}{\mu_k(\sigma_d)}d\tau$. For a step application of stress $\sigma$ maintained from $t = 0$, the two formulas can be totally identical by assuming that

$$\frac{\mu_k(\sigma_d)}{E_K} = \frac{n}{\alpha_T}[ln(\frac{\sigma}{\sigma_d})]^{n-1}. \tag{2.20}$$

Suppose $\mu_k(\sigma_d)$ follows a power law:

$$\mu_k(\sigma_d) = \frac{1}{K\sigma_d^{n-1}}. \tag{2.21}$$

The strain of the Kelvin unit can be expressed by either the spring or the dashpot element:

$$\epsilon = \frac{\sigma_s}{E_K} = \frac{\sigma - \sigma_d}{E_K}$$

or

$$\dot{\epsilon} = \frac{\sigma_d}{\mu_k(\sigma_d)} = K\sigma_d^n.$$

Solving these equations yields:

$$\epsilon(t) = \frac{\sigma}{E_K}\{1 - [(n-1)\frac{E_K}{\mu_{K0}}t + 1]^{\frac{1}{n+1}}\}, \tag{2.22}$$

where, $\mu_{K0}$ is the viscosity at $t = 0$.

An expedient computational solution for the delayed elastic creep strain can be obtained. Instead of making the current stress and strain under variable stress conditions a function of the entire past stress and strain history, the current stress of the dashpot is stored in the spring of the Kelvin unit. With this method, at the beginning of each time increment, only the stresses, strains and other parameters stored as state variables in the previous step need to be read and at the end of the increment, the new results calculated in this step are updated for the program to read at the beginning of next step.

In order to implement the finite element analysis, equations and parameters in the Burgers model are further simplified. Assuming that the strains of both dashpots follow the power law relation with respect to stress, the delayed elastic and secondary creep strain are as followings:

$$\dot{\epsilon}^d = \sigma/\mu_k = \dot{\epsilon}_0^d(\sigma_d/\sigma_0)^n \tag{2.23}$$

and

$$\dot{\epsilon}^c = \sigma/\mu_m = \dot{\epsilon}_0^c(\sigma_c/\sigma_0)^n, \tag{2.24}$$

where $\dot{\epsilon}_0^d$ and $\dot{\epsilon}_0^c$ are creep reference rates or creep parameters. The symbols $\mu_k$ and $\mu_m$ are the viscosity coefficients of the Kelvin and Maxwell units, i.e.,

$$\mu_k = (\sigma/\dot{\epsilon}_0^d)(\sigma_0/\sigma^d)^n \tag{2.25}$$

and

$$\mu_m = (\sigma/\dot{\epsilon}_0^c)(\sigma_0/\sigma^c)^n. \tag{2.26}$$

The dashpot in the Kelvin unit will carry most of the stress at the beginning for a very short time in a rapid loading. The elastic effect decreases with time and eventually creep will dominate. The above equations are dealing with uniaxial stress states only. In the case of multi-axial stress states, the general equation for ice deformation takes the following form:

$$\epsilon_{ij} = \epsilon^e_{ij} + \epsilon^d_{ij} + \epsilon^c_{ij}. \tag{2.27}$$

The elastic theory for multi-axial states is:

$$\sigma_{ij} = (K - \frac{2}{3}G)\epsilon^e_{kk}\delta_{ij} + 2G\epsilon^e_{ij}. \tag{2.28}$$

For the delayed and secondary creep strain, the strain and stress are divided into deviatoric and volumetric components, i.e.,

$$\sigma^d_{ij} = s^d_{ij} + \frac{1}{3}\sigma^d_{ii}, \tag{2.29}$$

$$\epsilon^d_{ij} = e^d_{ij} + \epsilon^d_v, \tag{2.30}$$

$$\sigma^c_{ij} = s^c_{ij} + \frac{1}{3}\sigma^c_{ii} \tag{2.31}$$

and

$$\epsilon^c_{ij} = e^c_{ij} + \epsilon^c_v. \tag{2.32}$$

More assumptions are made in the case of complex multi-axial stress conditions. These are as followings.

1. Ice creep is entirely deviatoric and its response to volumetric stress is elastic. There will be no volumetric deformation in creep except dilatation caused by cracking.

2. Shear strain follows the same power law as strain in the principal directions.

3. The viscosity coefficient is a function of the von Mises stress.

Based on these assumptions, the delayed and secondary creep deformation behaviour of multi-axial stress state can be described by:

$$\dot{e}_{ij}^{d} = \frac{2}{3} s_{ij}/\mu_k \tag{2.33}$$

and

$$\dot{e}_{ij}^{c} = \frac{2}{3} s_{ij}/\mu_m, \tag{2.34}$$

where the viscosity coefficients are:

$$\mu_k = (s/\dot{\epsilon}_0^d)(\sigma_0/s^d)^n \tag{2.35}$$

and

$$\mu_m = (s/\dot{\epsilon}_0^c)(\sigma_0/s)^n. \tag{2.36}$$

Introducing the von Mises stress $s = (\frac{3}{2} s_{ij} s_{ij})^{1/2}$ and equivalent strain $e = (\frac{2}{3} e_{ij} e_{ij})^{1/2}$ into the above equations (Xiao, 1991), the final solutions of the Burgers model are expressed entirely in terms of von Mises stress and the corresponding equivalent shear strain:

$$\dot{e}_{ij}^{d} = \frac{3}{2}\dot{\epsilon}_0^d (\frac{s^d}{\sigma_0})^n \frac{s_{ij}}{s} = \frac{3}{2}\dot{\epsilon}_0^d (\frac{s - E_k e^d}{\sigma_0})^n \frac{s_{ij}}{s} \tag{2.37}$$

and

$$\dot{e}_{ij}^{c} = \frac{3}{2}\dot{\epsilon}_0^c (\frac{s}{\sigma_0})^n \frac{s_{ij}}{s}. \tag{2.38}$$

The accumulated delayed elastic equivalent strain is obtained by integration:

$$e^d = \int_0^t \dot{e}_d dt = \int_0^t \dot{\epsilon}_0^d (s^d/\sigma_0)^n dt. \tag{2.39}$$

Following Sinha, $E_k = d/(c_1 d_1)$, $c_1 = 9$, $d_1 = 0.001m$ and $d$ is the grain size.

## 2.2 Damage Law

### 2.2.1 Ice Cracking

Ice is an extremely brittle material. Ice cracking is associated with the release of elastic strain energy. The brittleness of ice can be appreciated by its low values of fracture toughness, approximately 150–200 $KPa\ m^{1/2}$ which is of the same order as glass. Because of this property, for ice cracking to occur, very little energy is needed. As an ice sample is stressed, strain energy is stored. The energy is dissipated by viscoelastic movements and converted to surface energy. In the calculation made by Jordaan and Timco (1988), the energy for creating fracture surfaces is about 0.1% of the total energy dissipated in the indentation process. The remainder is believed to be consumed by relative viscoelastic movement between ice particles, which is thought to be a frictional process. Cracks can be divided into tensile cracks and compressive cracks according to the stress fields they are in. A critical stress level is necessary for both kinds of cracks to occur. Schulson (1989) shows that the critical stress for a tensile crack is:

$$\sigma_N = \sigma_0 + kd^{-1/2} \tag{2.40}$$

where $\sigma_0$ and $k$ are constants and $d$ is the ice grain size. The mechanism of compressive cracking is very complicated. Attention is focused on compressive cracks (Figure 2.6) in the following. The average crack size is about 0.65 times the average grain size. The crack size is independent of stress while the crack density is a function of stress. Even under multiaxial stress states, as observed by Kalifa (1989), the cracks in ice tend to form in the direction of highest principal compressive stress.

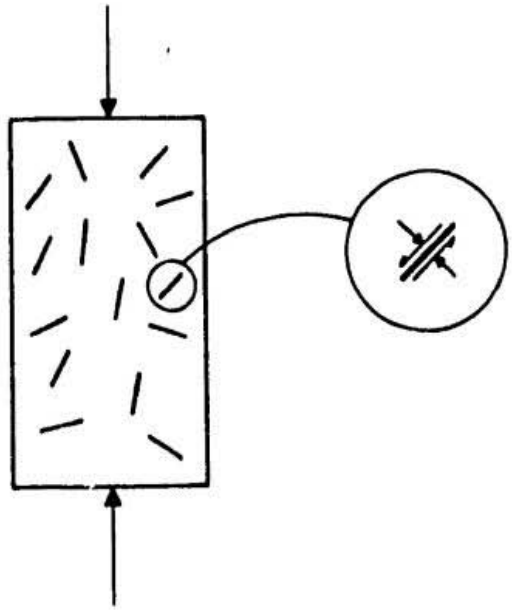

Figure 2.6: Compressive Cracks

### 2.2.2 Damage Evolution

Ice indentation tests show the evidence of the development of microcracks along the maximum shear stress (Figure 2.7). The failure of the ice could be described by three stages:

1. Elastic deformation with no cracks.

2. Nucleation of microcracks and increasing crack density with stress.

3. Failure stage, loss of resistance to any stress or stabilized stress-strain relation due to high level of damage caused by high density of cracks.

According to the damage level, the ice sheet ahead of an indentor can be characterized by three zones (Figure 2.8):

1. Virgin ice, undamaged or intact ice

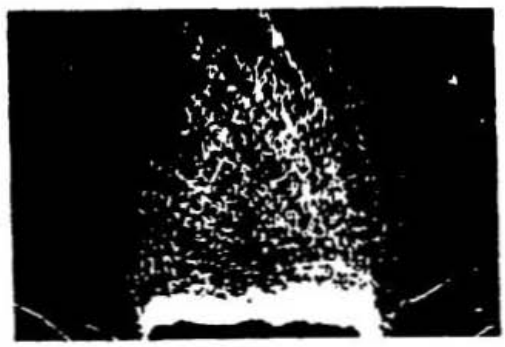

Figure 2.7: Ice Cracks Ahead of an Indentor (Jordaan and Timco, 1988)

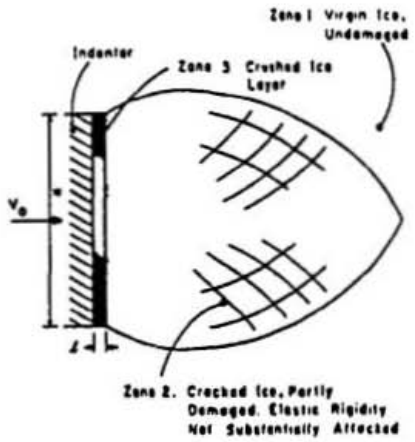


Figure 2.8: Three Zones of Damage (Jordaan and Timco, 1988)

2. Partly damaged ice with high density of cracks

3. Totally damaged or crushed ice

The critical zone is very important in ice force calculation because it will carry most of the load. The critical zone effect will be discussed in detail later. The crushed ice can still stand some compressive stress due to its frictional properties.

Under the damage condition, the constitutive models in the last section can not be used directly without including the effect of the damage. Damage mechanics is therefore applied to ice modelling.

The process of damage is defined as the accumulation of micro-defects inside the ice structure. As mentioned above that the compressive cracks tend to be oriented in the direction of the highest principal stress, a scalar representation D is used as a damage parameter. Figure 2.9 shows a body with an overal sectional area of $A_0$ and a damage area of A. With uniaxial stress P, the effective stress of this damaged body is:

$$\sigma_a = \frac{P}{A_0 - A} = \frac{P}{A_0(1-D)} = \frac{\sigma}{1-D}, \tag{2.41}$$

and the elastic deformation is:

$$\epsilon = \frac{\sigma_a}{E_0} = \frac{\sigma}{E_0(1-D)} = \frac{\sigma}{E} \tag{2.42}$$

where $\sigma_a$ is the effective stress; $E_0$ is the elastic modulus and $E$ is the effective modulus. The damaged ice can be considered equivalent to intact ice provided that the virgin elastic modulus is replaced by the effective elastic modulus. The

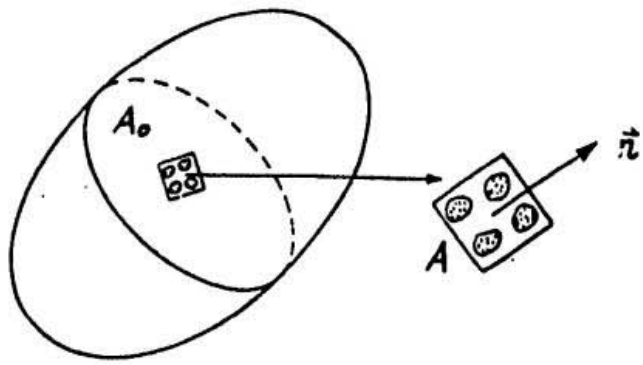


Figure 2.9: The Overall Area and the Damage Area (Xiao, 1991)

development of damage depends on the stress, strain and the current damage degree (Xiao, 1991):

$$D = f(e, \dot{e}, \sigma, \dot{\sigma}, D, ...\dot{D}). \tag{2.43}$$

The degree of damage is simply represented by a damage parameter (Xiao, 1991):

$$D_N = a^3 N, \tag{2.44}$$

where $a$ is the radius of crack surface which, for simplicity, is chosen to be the grain size and $N$ is the crack density. To get the crack density $N$, a damage evolution analysis has to be done. Following Jordaan, McKenna and Xiao (1990), a rate expression of crack nucleation rate is given:

$$\dot{N} = \dot{N}_0(\frac{s}{\sigma_0})^m, \tag{2.45}$$

where the $N_0$ is a damage constant; s is the overall stress; $\sigma_0$ is a reference stress of 1 MPa and m is a damage exponent.

The damage theory and its applicability to ice was mentioned by Schapery in 1991. The damage measurement given by Schapery (1991) is:

$$S_\sigma = \int_0^t (\frac{s}{\sigma_0})^q dt' \tag{2.46}$$

where $S_\sigma$ accounts for the accumulation of damage, $s$ is the overall stress and $q$ is a constant. $S_\sigma$ could also be expressed as:

$$\dot{S}_\sigma = S_0(\frac{s}{\sigma_0})^q \tag{2.47}$$

where $S_0$ is a constant. Schapery's approach make it possible to consider all kinds of damage in one measurement. In the following analysis, Schapery's expression of damage is adopted.

### 2.2.3 Damage Effects

Damage induces a change in ice structure integrity resulting in a weakening by reducing the effective modulus and stiffness. The change of elastic properties is determined by calculating the loss of strain energy due to the formation of cracks. The equations of the change of elastic properties are given by Budiansky and O'Connell (1976). By using the damage parameter given by Xiao (1991), their equations become:

$$K/K_0 = 1 - \frac{16(1-\nu^2)}{9(1-2\nu)} D_N \tag{2.48}$$

and

$$G/G_0 = 1 - \frac{32(1-\nu)(5-\nu)}{45(2-\nu)} D_N \tag{2.49}$$

where $K$, $G$ and $\nu$ are the cracked bulk and shear moduli and cracked poisson ratio respectively. The subscript "0" denotes the intact ice properties. Figure 2.10 shows the change of elastic modulus in uniaxial stress test (Xiao, 1991). Based on Horri and Nemat-Nasser (1983) and Xiao (1991), Budiansky and O'Connell's equation can be simplified and modified to:

$$G/G_0 = 1 - \omega D_N \tag{2.50}$$

$$K/K_0 = 1 - \omega D_N, \tag{2.51}$$

where $\omega = 16/9$ in tension and $\omega = 1$ in compression since the reduction of elasticity is smaller.

In the above formulas, the interaction between cracks is considered but the traction effect across the crack surfaces, which is very important in high confining pressure situation, is not included. The solution is only valid in the case where the cracks remain open. Under compression, as will be discussed later in next chapter, the crack effects on ice elastic properties will be reduced due to the difficulty in crack nucleation and the closure of cracks.

The effects of damage on creep are more significant. Figure 2.11 shows the strain-stress curves of the uniaxial test results for both intact and predamaged ice. The creep strain of damaged ice is about 5 to 10 times of that of intact ice. Jordaan et al. (1988) found that when the damaged ice creep is enhanced by a factor of 10, the reduction of the Young's modulus is only 10 percent.

As shown in equations 2.33 and 2.34, the representations for primary and secondary creep of the intact ice take the same form. The Glen's law in uniaxial

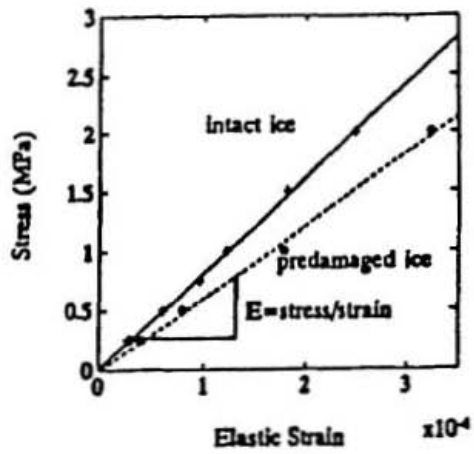


Figure 2.10: Elastic Behaviour of Intact and Damaged Ice (Xiao, 1991)

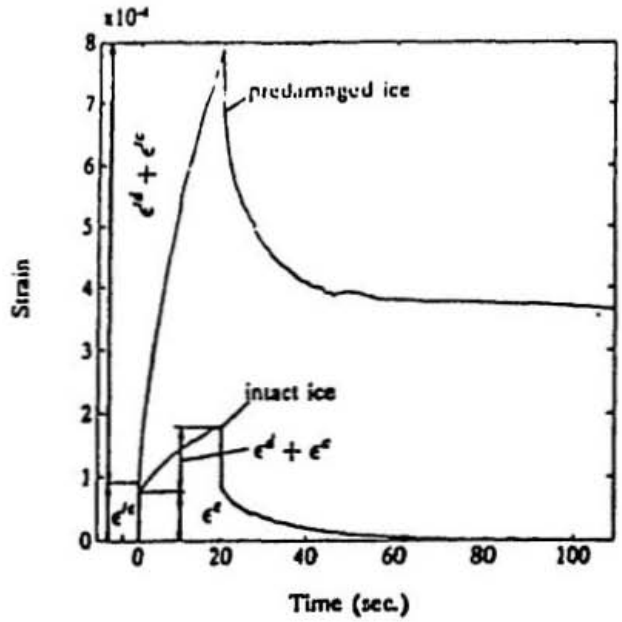


Figure 2.11: Strain Response of Intact and Predamaged Ice for Constant Stress ( Xiao, 1991)

damage state $S_\sigma$ can be generalized to:

$$\dot{\epsilon} = f(S_\sigma)\sigma^n, \tag{2.52}$$

where the damage is assumed to result in a reduction in cross-section with a corresponding increase in stress. An exponential form is introduced by Jordaan and McKenna (1988) for damage models of both primary and secondary creep:

$$\dot{e}^{d\prime}_{ij} = \dot{e}^{d}_{ij} exp(\beta_d S_\sigma) \tag{2.53}$$

$$\dot{e}^{c\prime}_{ij} = \dot{e}^{c}_{ij} exp(\beta_c S_\sigma), \tag{2.54}$$

where the primes refer to strain rates of the cracked ice; $\beta^d$, $\beta^c$ are constant enhancement parameters; and $\dot{e}^{d}_{ij}$, $\dot{e}^{c}_{ij}$ are strain rates for intact ice which, for instance, can be represented by Burgers Model. Creep enhancement is found both in uniaxial and triaxial stress states. The percentage of elastic strain in total deformation becomes smaller and smaller with the increase of damage. Creep will dominate the total strain under high damage condition.

# Chapter 3

# Influence of Hydrostatic Pressure on Ice Deformation

Evidence shows that the hydrostatic part of the stress tensor is also very important in ice deformation under triaxial stress. If the total deformation is divided into a deviatoric and a volumetric component, the hydrostatic pressure will have an effect not only on the volumetric but also on the deviatoric component.

The hardening and softening effects of hydrostatic pressure are discussed in this chapter. Pressure hardening effects will make cracks more difficult to nucleate; suppress the elastic failure and increase ice stiffness by closing cracks which already exist. Pressure softening effects will reduce the viscosity of ice and the friction at crack interfaces. The pressure softening effects may be caused by pressure melting and dynamic recrystallization.

## 3.1 Pressure Hardening - Crack Suppression

### 3.1.1 Effect of Hydrostatic Stress on Crack Nucleation

Kalifa et al. (1989) explain the crack nucleation as a stress-induced process at the head of a pile-up. In their study, the first crack forms at a uniaxial compressive

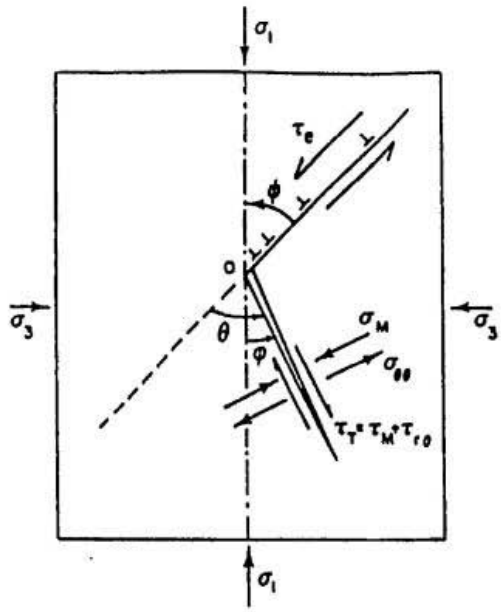


Figure 3.1: Two Stress Fields Acting on a Nucleated Crack (Kalifa et al., 1989)

approximately 2 MPa.

Figure 3.1 shows stresses on a nucleated crack at the head of a pile-up under triaxial compressive stress field. Two stress fields are assumed to act on the crack: the local stress field induced by the dislocation pile-up process and the remote stress field. Based on this assumption, the local tensile stress field and the remote stress field will contribute to the two components of the mode I stress intensity factor for crack nucleation. According to Kalifa et al., the stress intensity factor is:

$$K_I = K^l + K^e, \tag{3.1}$$

where $K^l$ represents the local tensile stress component which drive the crack to open and $K^e$ is the remote stress component which inhibits the crack growth.

Through the stress analysis, it is obtained that

$$K_I = -\sigma_1(\pi d)^{1/2} F_I, \tag{3.2}$$

where:

$$F_I = \frac{3}{4}(1-\lambda) sin2\psi \, sin\theta \, cos\frac{\theta}{2} - (\frac{d}{l})^{-1/2}(1+(\lambda-1)cos^2\phi) \tag{3.3}$$

where

$l$ is the microcrack length and is comparable to the grain size,

$d$ is the pileup length,

and $\lambda$ is the confining coefficient and equals $\sigma_3/\sigma_1$.

If a crack forms, $K_I$ must equal the fracture toughness $K_{Ic}$. The resulting criterion for critical shear stress at the crack formation is:

$$\sigma_1 - \sigma_3 = -\frac{K_{Ic}}{(\pi d)^{1/2} G_I}, \tag{3.4}$$

where:

$$G_I = (\frac{d}{l})^{-1/2} sin^2\theta - \frac{3}{4} sin2\psi \, sin\theta \, cos(\frac{\theta}{2}). \tag{3.5}$$

Kalifa et al. (1989) also used triaxial tests to study the effect of hydrostatic stress on critical stress and strain for crack nucleation. The results of their tests were regressed by the least squares method giving the following equation,

$$\sigma_1 - \sigma_3 = -2.47 + 0.4\sigma_3. \tag{3.6}$$

The theoretical (dotted line) and experimental (solid line) equations are shown in Figure 3.2.

Through the theoretical derivation of the equation for crack formation under compressive stress fields, an important finding was that crack formation is dominated by the remote stress field whereas the local tensile stress field generated by

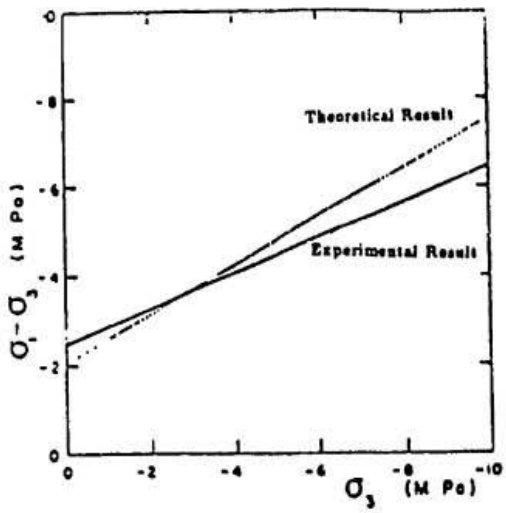


Figure 3.2: Theoretical and Experimental Critical Differential Stress as Function of Confining Stress (Kalifa et al., 1989)

dislocation pileup has little effect. A very noticeable feature is the clear increase of the critical crack initiation stress with confining pressure. Within the range of their tests, the critical stress for crack nucleation is increased from about 2 MPa in uniaxial loading to 6.5 MPa in triaxial loading with a hydrostatic stress of 10 MPa. Under even higher confinement, for instance, 25 MPa, which is often encountered in medium scale indentation tests and full scale interactions, very high deviatoric stress is needed to initiate a crack. The critical strain is also found to increase with hydrostatic pressure, that is resonable considering the increase of stress. It is interesting that the elastic strain component decreases as the total critical strain increases with confinement. This indicates that the first crack nucleates in a deformation condition more and more characterized by ductile response with the increase of confinement. This phenomenon and the bigger stress and strain needed to create cracks will certainly delay the early occurence of cracks and prevent the

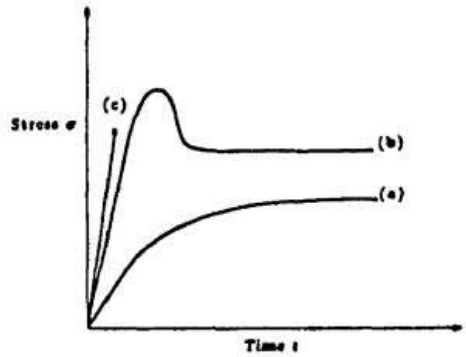


Figure 3.3: The Response of Ice in Uniaxial Compression at (a) Low (b) Intermediate and (c) High Rates of Loading (Cocks, 1988)

ice from failing due to brittle shearing and splitting.

### 3.1.2 Effect of Hydrostatic Stress on the Failure Mode of an Ice Sample

The majority of the ice tests are uniaxial compressive. Figure 3.3 shows the response of ice samples loaded in uniaxial compression at different strain rates. Tests were done at low, intermediate and high strain rates. The high strain rate deformation of uniaxial compressive ice (c) is characterized by an elastic increase of stress, followed by a brittle failure caused by crack propagation. A brittle solid in such uniaxial compression might be expected to fail by axial splitting alone, as cracks propagate parallel to the principal stress direction (Ashby and Hallam, 1986). The shear fracture observed by Schulson (1987) and Rist et al. (1988) is attributed to the end effect (Rist el al., 1988). The ends of the tested ice sample are fixed

by the testing equipment which exerts frictional constraint on the ice sample. The expected axial splitting is inhibited at the ends especially at high strain rates where the frictional force is sufficient to prevent the axial fractures from propagating the entire specimen length.

The confining pressure superposed on the uniaxial test has the same effect as the ends. Under moderate confining pressures, failure might occur by shear fracture, independent of specimen ends. The process of axial splitting and shear faulting is predominantly a function of confinement (Horii and Nemat Nasser, 1985). As shown in Figure 3.4, in the case of axial splitting (left figure), a single fracture associated with wing cracks propagates throughout the ice specimen. On the other hand, the accumulated deformation under increasing confinement will make the cracks coalesce, resulting in the formation of a shear fault. As seen in the right figure in Figure 3.4, a family of stable wing cracks coalesced along the shear fault surface and a matrix of coarse and fine powdered material was created.

Further increment in confinement will suppress this brittle failure leading to a higher stresses and failure due to visco-elastic flow. Recent work done by Murrell, Sammonds and Rist (1990) also showed the same tendency. Under triaxial compression at low temperature and high strain rates, shear fracture is reduced and finally eliminated as the confining pressure increases. They attribute this elimination of shear cracks to the increased difficulty of nucleation or propagation of cracks in triaxial compressive stress field. Figure 3.5 and Figure 3.6 show the stress-strain curves under hydrostatic pressures of 1.2 MPa and 30 MPa respectively.

In conclusion, two transitions might be identified. First, from very low to moderate hydrostatic confining pressure, there is a transition from tensile axial

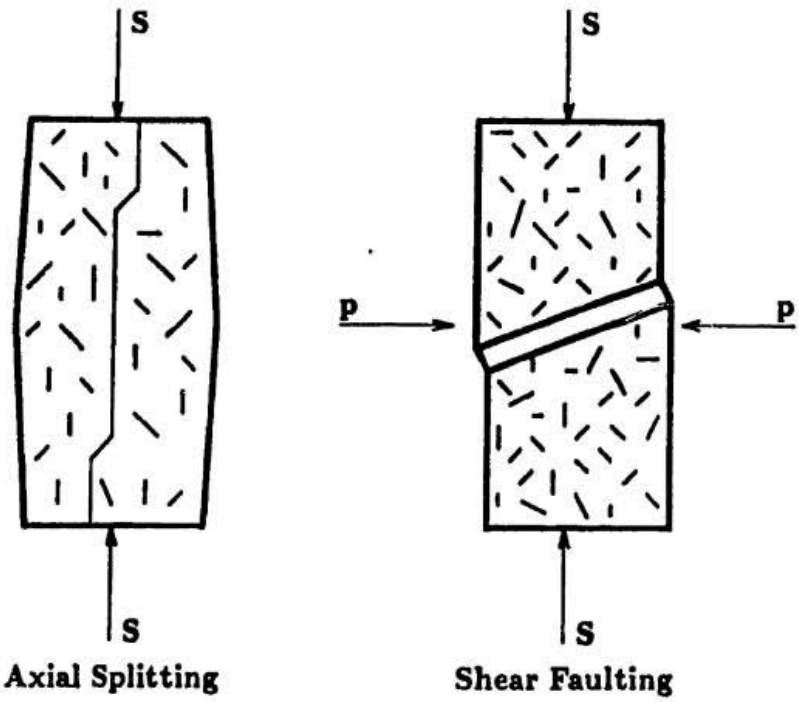


Figure 3.4: Axial Splitting and Shear Fracture (Kenny, 1992)

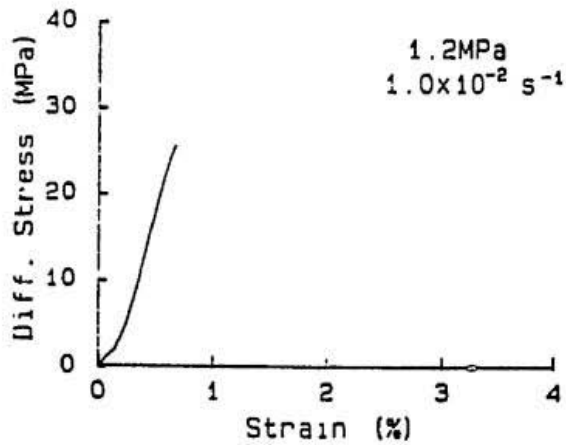


Figure 3.5: Stress-Strain Curve with Hydrostatic Pressure of 1.2 MPa and Strain Rate of 0.01/s (Murrell and Others, 1990)

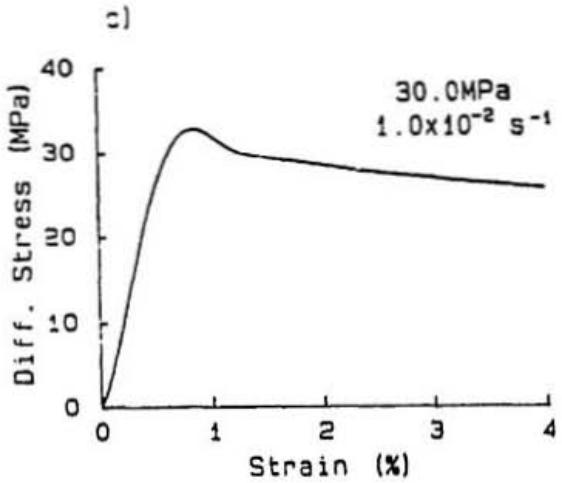


Figure 3.6: Stress-Strain Curve with Hydrostatic Pressure of 30 MPa and Strain Rate of 0.01/s (Murrell and Others, 1990)

splitting to shear fracture. Second, from moderate to high hydrostatic confining pressure, there is a transition from shear fracture to visco-elastic flow. The second transition is more profound because it indicates a change in failure mechanism, i.e. from crack propagation to creep enhanced by microcracking.

At low strain rates, the ice responds in a ductile manner under any confining pressure and therefore the hydrostatic pressure does not have as much effect. In other words, it does not change the failure character at early stage of deformation. This can be seen in Figure 3.7 and Figure 3.8 where strain rates are one order of magnitude lower than in Figure 3.5 and Figure 3.6.

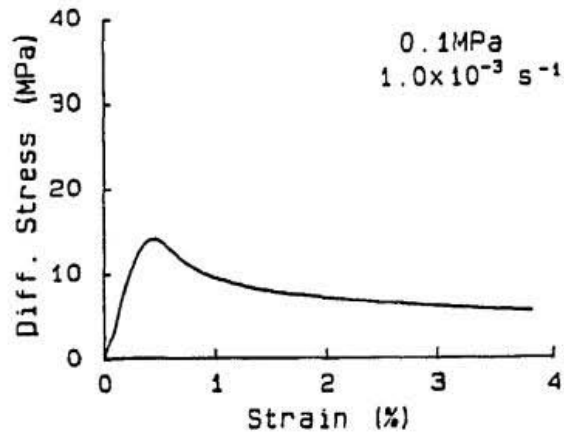


Figure 3.7: Stress-Strain Curve with Hydrostatic Pressure of 0.1 MPa and Strain Rate of 0.01/s (Murrell and Others, 1990)

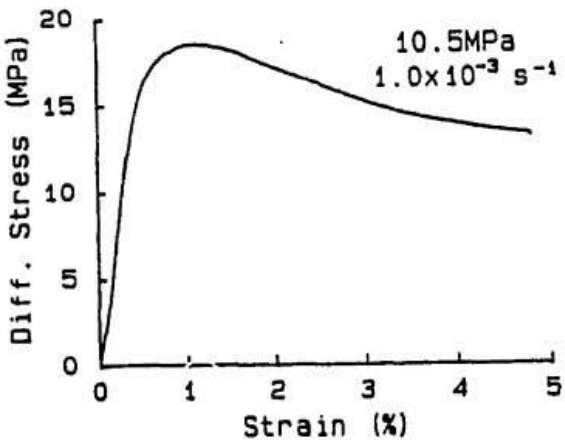


Figure 3.8: Stress-Strain Curve with Hydrostatic Pressure of 10.5 MPa and Strain Rate of 0.01/s (Murrell and Others, 1990)

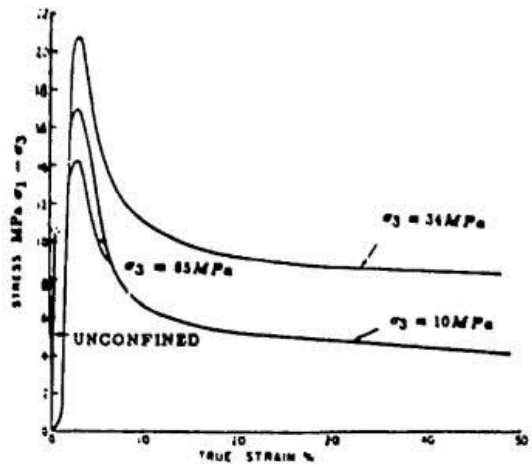


Figure 3.9: Stress-Strain Curves of Polycrystalline Ice for Various Confining Pressures (Jones, 1982)

### 3.1.3 Effect of Hydrostatic Stress on the Development of Damage

Temperature, strain rate and confining stress have great effects on the process of ice deformation under triaxial stress states. The peak stress will increase with strain rate and decrease with temperature. Hydrostatic stress has little effect on the peak stress at low strain rates in the order of $10^{-6}$ because ice creeps in both confined and unconfined tests with little cracking. However, ice deformation at low strain rates is not very important in most ice force because most deformation rates in real interaction cases are around $10^{-3}s^{-1}$ or higher. The attention of the confining pressure effect on compressive behaviour of ice will be focused on the high strain rate regime.

Figure 3.9 shows the stress strain curves under triaxial stress condition (Jones, 1982). All tests were carried out at temperature of $-11°C$ and at strain rate of 5.5*

$10^{-3}s^{-1}$. The short straight line is the result of the test conducted under uniaxial stress. This is an elastic deformation followed by a brittle failure. The change of mechanism from brittle failure to ductile creep with the increase of confining pressure has already been discussed in last section and is once again proved in this test. Up to confining stresses of 34 MPa, the peak stress increases with confining stress. The observed phenomenon strongly suggests that hydrostatic pressure might close or eliminate cracks pushing peak stress to a higher level. As the confining pressure increases, neither multiple axial splitting nor shear fracture is possible. The failure is caused by the increasing density and the interaction of cracks. The creep is greatly enhanced by this kind of damage (see Chapter 2). The increasing hydrostatic stress may stop or slow down this enhancement and make the ice hold longer before failure. In Figure 3.9, when the confining pressure is 85 MPa, the peak stress drops. This is caused by pressure melting (Jones, 1982) and will be discussed in detail later in this chapter.

Gold (1972) explains the behaviour of ice around the peak pressure with a transition theory. The extensive network of cracks causes the specimen to lose resistance to deformation. At a certain moment (when failure starts), creep is accelerated from the primary stage directly to tertiary behaviour. Jones (1982) points out that the transition strain rate increases with confining pressure. If other conditions are the same, when the stress of a less confined test levels off, the stress of a more confined test will continue to rise because the confinement pushes the transition zone to a high level of stress and strain rates. The higher the confining pressure, the higher is the deviatoric stress needed to initiate a crack or to increase crack density.

In both uniaxial and triaxial tests, the deviatoric stress peaks and then drops to a lower value, which is maintained with increasing strain. This low value of stress is referred to as the post peak stress. Some test results show that this post peak stress increases with hydrostatic pressure. It is also observed that the difference between the peak stress and post peak stress decreases with confining pressure which implies that the increase of post peak stress with confining pressure is faster than the increase of peak stress though both of the increases are very small. Since the confining stress may play an important role and contribute a significant portion of the deformation resistance of the ice sample, the differential stress would drop more sharply with the release of the confinement.

In almost all the triaxial stress tests, the confining pressures are held constant throughout the tests. When the stress peaks and drops, the confinement is unchanged and its effect remains. On the other hand, in indentation tests and full scale interactions, the drop of the load is often accompanied by a quick release of confinement due to extrusion. To simulate the real process of failure, hydrostatic stress should be released when the stress drops. A sharper drop of stress and a bigger difference between peak and post peak stress might be expected.

It is concluded from the above analysis that the development of damage is inhibited by the high hydrostatic pressure. The damage evolution law should be a function of both shear stress (von Mises stress here) and volumetric stress. A pressure effect factor $F(p)$ could be simply put into the damage law:

$$\dot{S}_\sigma = S_0(\frac{s}{\sigma_0})^q F(p), \tag{3.7}$$

where $F(p)$ is a function of hydrostatic pressure $p$. The bigger the hydrostatic pressure, the smaller the damage rate. The following form of $F(p)$ is used in

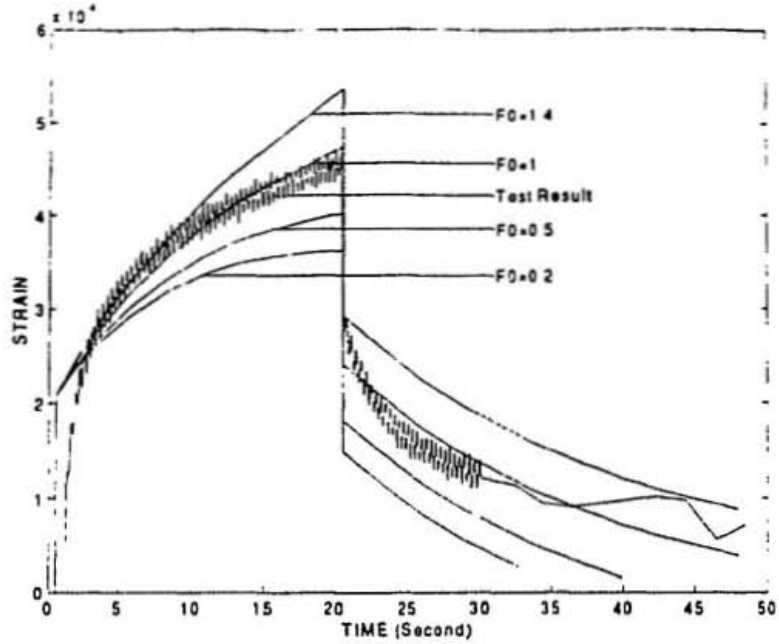


Figure 3.10: Test and Model Results of the Triaxial Test

example simulations in Chapter 5:

$$F(p) = F_0(\frac{p_0}{p})^f \tag{3.8}$$

where $F_0$ and $f$ are constant. To illustrate, constant stress test conducted under triaxial compressive stress (Stone and Xiao, 1993), is modelled by using equation 3.7 and 3.8. The hydrostatic pressure is 10 MPa and the differential stress is 1 MPa. The test result and the model results are shown in Figure 3.10. The constant $f$ is assumed to be 1 and different values of $F_0$ have been tried to fit the test result. It is seen from Figure 3.10 that the strain decreases with $F_0$. The decrease of $F_0$ is equivalent to the increase of pressure hardening effects. Ice becomes harder when more pressure hardening effects are considered.

## 3.2 Pressure Softening Effects

### 3.2.1 Pressure Melting and Ice Friction

The melting point of ice is depressed by hydrostatic pressure. A general solution (the Clausius Clapeyron equation) is given for one substance with two phases at phase equilibrium:

$$\frac{\partial P}{\partial T} = \frac{L}{T(v_l - v_s)}, \tag{3.9}$$

where P and T are pressure and temperature; L is the latent heat and $v_l$ and $v_s$ are specific volume of liquid and solid phases respectively. The variation of melting temperature with pressure is determined from this equation. A simple calculation using this equation (Barnes et al., 1971) yields a result at an equilibrium temperature of $273K$:

$$dT_m = -0.074°C/MPa, \tag{3.10}$$

i.e. a pressure of about 13.5 MPa causes a depression of $T_m$ equal to $1°C$.

Nordell (1990) carried out an experimental study on pressure melting. His test results, along with the results of theoretical and experimental studies by other researchers, are shown in Figure 3.11. All results seem in good agreement with each other. A rough estimate made by Jones (1982) is that to lower the melting point from $0°C$ to $-10°C$, a pressure of 110 MPa is required. While this is a relatively large pressure, it may actually be achieved in practise. In medium scale indentation tests, pressures up to 70 MPa have been recorded. Considering the stress concentrations on asperities and other high local pressure area, the pressure in the grain boundary at contact points could then be several times this value.

In the test performed by Barnes et al. (1971), a transition from creep to pressure melting was identified. Figure 3.12 shows the indentation hardness of polycrystalline ice as a function of absolute temperature for various loading times (Barnes and Tabor, 1971). Their test results provide evidence of a further deformation process at temperature within a degree or so of the melting point; the rate of flow of ice was much faster than that expected from creep process alone. They suggested that these occur when the contact pressure was sufficient to produce localized pressure melting. This can be seen in Figure 3.12, where the points to the left of the broken line show a marked drop in hardness. The broken line is the pressure-melting curve. Ice in the pressure melting regime is much softer. To the right-hand side of the pressure-melting curve, the flow of the ice is not influenced by pressure melting.

A very important feature affecting the friction between ice and ice is the existence and extent of any liquid layer between ice surfaces. Once the layer is formed, it will become the place where the relative movement takes place. The coefficient of friction is therefore dependent on the thickness of this layer. The thicker the layer, the smaller the friction. In a process of friction between ice surfaces, the amount of water generated by pressure melting and frictional heating increases with velocity and contact temperature. At the melting point, the friction coefficient drops dramatically. A decrease in friction coefficient with both velocity and temperature was observed in tests done by Barnes et al. (1971) as well as in tests done by Jones, Kennedy and Schulson (1991). Figure 3.13 shows the results obtained by Jones et al (1991).

In Figure 3.9, when a confining pressure of 85 MPa was used, the peak stress dropped. This indicates a different mechanism involved around the peak stress for

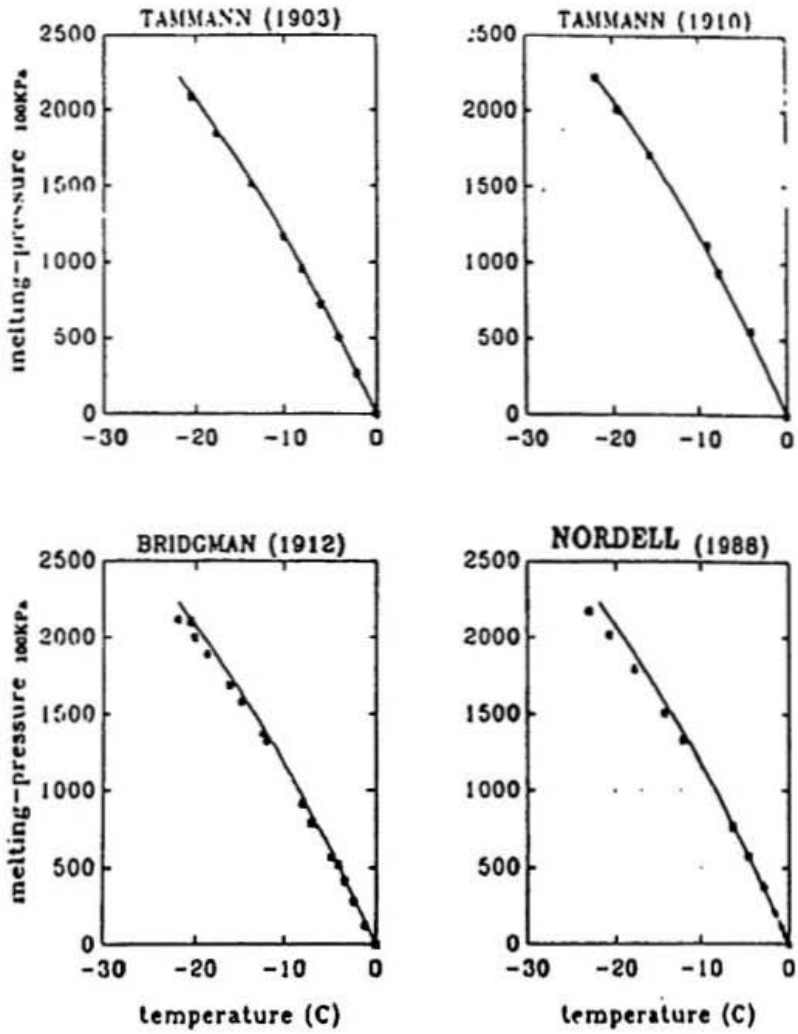


Figure 3.11: Melting Pressure and Temperature

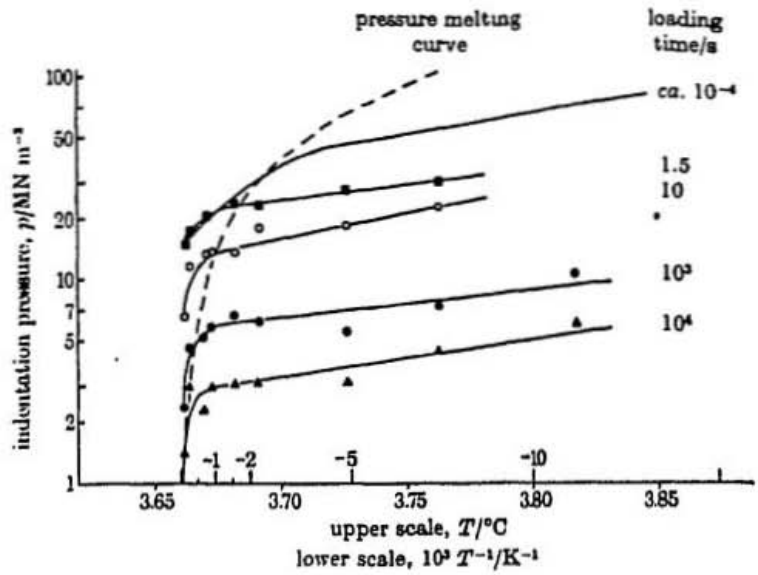


Figure 3.12: Indentation Hardness of Polycrystalline Ice as a Function of Absolute Temperature (Barnes et al., 1971)

very high confining pressures. As will be discussed later, the amount of liquid in grain boundaries will increase as the confining pressure increases. Pressure melting makes the ice less creep resistant. In the case where the global stress is less than that required for a phase change, pressure melting may be active on a localized level because of intense stress concentrations at crack tips or at triple junctions. If the confining pressure continues to increase, there will eventually be a phase change.

Pressure melting has been observed in the large scale indentation experiments performed in the multi-year sea ice at Hobson's Choice Ice Island in 1990 (Meaney et al., 1991). The rapid movement of the indentor in the time-displacement curve corresponds to the drop of load in time-load curve (the rapid and relatively slow movement are shown in Figure 3.14). The temperature variation has been registered during the fast and slow forward motion.

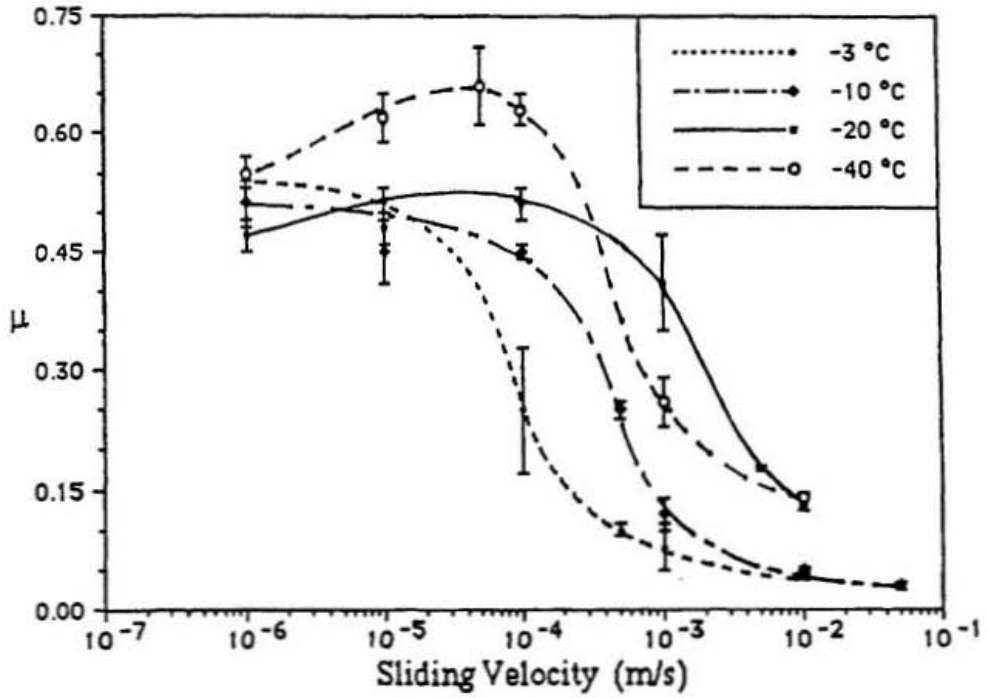


Figure 3.13: Kinetic Friction of Saline Ice at Different Velocity and Temperature (Jones et al., 1991)

In indentation tests, as the load increases, the pressure on hot spots might become high enough to cause melting, although the average pressure exerted on the total contact area is still low. Upon melting, the ice viscosity and friction between ice particles will reduce. The ice will rapidly lose strength and indentor will jump ahead suddenly, with damaged ice particles being extruded. The inertia of the rapidly moving indentor exerts further pressure on the remaining ice. The indentor then decelerates and eventually stops at the point that the ice sample is able to stand the load again. The load then begins to accumulate, starting the cycle again. Figure 3.14, for example, shows these regular cycles of load vibration.

For elastic materials, the relation of the strain energy $W$ with other energy is given by Jordaan and McKenna (1988) as

$$\dot{W}_e = \dot{W} + \dot{W}_d + G\dot{D}_N, \tag{3.11}$$

where $W_e$ is the work supplied by the external force; $W_d$ is the energy dissipated on internal crack surfaces i.e. dissipated by friction; $G$ is the strain energy release rate:

$$G = \partial W / \partial D_N \tag{3.12}$$

and the superimposed dots indicate rates with respect to time. Ice is a viscoelastic material which creeps and the energy dissipated by crack enhanced creep is also a big contributor to the energy consumed in the above equation. As will be discussed later, the slow friction between cracks under adhesion conditions also involves creep. During the slow indentor displacement, as the load builds up, creep and friction between cracks as well as other local relative movement such as grain structure

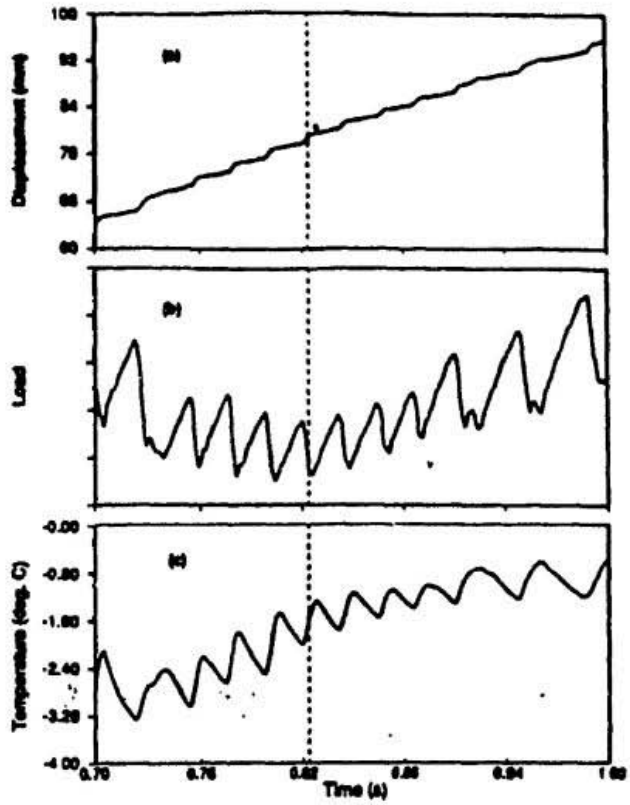


Figure 3.14: Corresponding Segments of Displacement, Load and Temperature (Gagnon and Sinha, 1991)

broken would consume most of the energy. In the downswing part of the load-time curve, viscous extrusion of the damaged ice in both low and high pressure areas would consume most of the energy. The extrusion of damaged ice particles is obviously dominated by frictional process. The energy transfer in the whole cycle of load variation is characterized by frictional dissipation. According to a rough calculation done by Jordaan (1988) for medium scale indentation test, equal amounts of the external work go into the upswing and downswing part of the loading and failure cycle.

Figure 3.14 shows the corresponding indentor displacement, load and temperature as a function of time recorded in Hobson's Choice Ice Island experiments (Gagnon and Sinha, 1991). From this figure, it is seen that the sudden drop in load and abrupt forward motion of indentor are accompanied by a rise of temperature. The following explanations are given by Gagnon and Sinha (1991). When the load drops, the mixture of ice particles and liquid are extruded. This process, which further relieves the pressure, can be described using viscous flow theory. As the pressure drops, the melted ice quickly refreezes, generating heat. As a result, the temperature increases. On the load building side of the load-time curve, the amount of water created by pressure melting increases with the hydrostatic pressure and the melting ice takes more and more heat from the surrounding ice at a lower pressure. As a result, the temperature drops.

### 3.2.2 Softening Effects Caused by Dynamic Recrystallization

When recrystallization is synchronous with deformation, it is called dynamic recrystallization. Dynamic recrystallization is an important process during deformation of many rock-forming minerals. It can strongly influence mechanical properties and the development of microstructure. A study of dynamic recrystallization for impure single-phase materials like calcite marble, quartzites, glacier ice, or single-phase regions of multi-phase rocks was done by Urai et al. (1986). Dynamic recrystallization may occur during ice deformation in indentation tests.

While several boundaries of a new grain may be established by grain boundary migration, full isolation of the grain may commonly be achieved by development of a bridging subgrain boundary and its conversion by progressive misorientation into

a grain boundary. The generation of new grains during dynamic recrystallization may occur on grain boundaries. The recrystallized grain size would be more or less equal to the optically visible subgrain size.

In most cases, the influence of dynamic recrystallization is a softening and creep enhancing effect. The fundamental processes responsible for this effect are changes in grain size, changes in substructure, changes in preferred orientation and changes in grain boundary structure. The softening and creep enhancing effect is a combination of these processes.

Bouchez and Duval (1982) mention increases of up to an order of magnitude in strain rate in ice tests associated with the increased number of grains with the same slip orientation due to dynamic recrystallization. Another evidence they give is that the coefficient of diffusion in a migrating grain boundary can be much higher than in a stationary one (no recrystallization). Because of this effect, the contribution of diffusion assisted grain boundary sliding to the total strain may strongly increase and the material may be weakened.

It is believed that ice grains might be broken down under high hydrostatic pressures during an indentation process. A fine grain ice structure was found at the hot spots at the Hobson's Choice Ice Island indentation tests. Recrystallization is a possible mechanism. A strong decrease in grain size by recrystallization can result in a change in the dominant deformation mechanism to diffusive mass transfer. This in turn should result in a weakening of the material.

The growth of new grains causes a sudden weakening. In a test of polycrystalline material (Urai, 1983), it was found that during steady state flow at high confining pressure, dynamic recrystallization occurred and recrystallization resulted in a de-

crease of the creep stress by about a factor of two. It was also found in this test that when hydrostatic pressure is higher than 28 MPa, the creep stress begins to decrease with the hydrostatic pressure. Urai (1986) explained the test results with the decrease in dislocation density across the interface caused by strain-induced migration of grain boundaries. Dynamic recrystallization also provides more volume of grain boundary for pressure melting water. The melting water will reduce the friction at the interfaces of ice particles. The test results of Urai (1983a) show that the creep stress of the wet material is much lower than that of dry material under the same stress condition. It is therefore concluded that the dynamic recrystallization might be a reason for pressure softening effects in ice deformation.

### 3.2.3 Ice Model and Pressure Melting Effects in Indentation Tests

Two systems of ice have been defined by Jordaan and McKenna (1991), first, the solid body, i.e. the parent viscoelastic material, and second, the cracks, along with the thin layer adjacent to the crack surfaces.

Cracks will form soon after loading when grain boundary sliding starts. In the initial stage of crack propagation, there are several local events in a thin layer adjacent to the crack faces. These local events are characterized by friction dissipation accompanied by adhesion, bond breaking, bond crushing and by stress concentration on asperities. The role played by compression and shear between crack surfaces can not be neglected, in particular considering the increasing number of cracks with damage progress.

Based on Barnes et al. (1971), the friction between ice and ice at low frictional speeds is similar to the creep behaviour of ice. Some shear strain and stress curves

are given in Figure 3.15. If the friction between crack faces is viewed as shear of the thin layer adjacent to the two faces (Barnes et al., 1971), these strain and stress curves can be used to describe the local frictional movement at low strain rates of ice deformation in indentation. Figure 3.15 gives the damaged enhanced creep, sliding friction and pure secondary creep curves obtained by Stone et al. (1989), Barnes et al. (1971) and Sinha (1982). One can see from these results that the frictional behaviour between cracks is similar to that of the enhanced creep of the parent viscoelastic ice as a whole. The enhancement in friction corresponding to the creep enhancement by damage is the result of recrystallization. Thus the lower part of the damage enhanced creep curve can well apply to slow relative movement between ice and ice when the adhesion is important. This movement across the crack faces would not affect the strain energy significantly. During the relatively slow motion of an indentor, the viscoelastic model and damage law can be used to model both the solid parent ice and local cracked ice. The application of this model to the simulation of an indentation test is implemented through the finite element method (Xiao, 1991). Good agreement between the model and the test results has been obtained.

In Figure 3.15, the sliding friction curve obtained by Barnes et al. (1971) shows that when the shear strain rate increases and reaches a certain level, the shear stress stops increasing and starts to decrease. This phenomenon is associated with the generation of water due to pressure melting during the tests. More water is expected in a triaxial stress test with high confinement pressure because of the significant role played by pressure melting. The water generated by frictional heating and pressure melting would first reduce the viscosity of the thin layer adjacent to crack

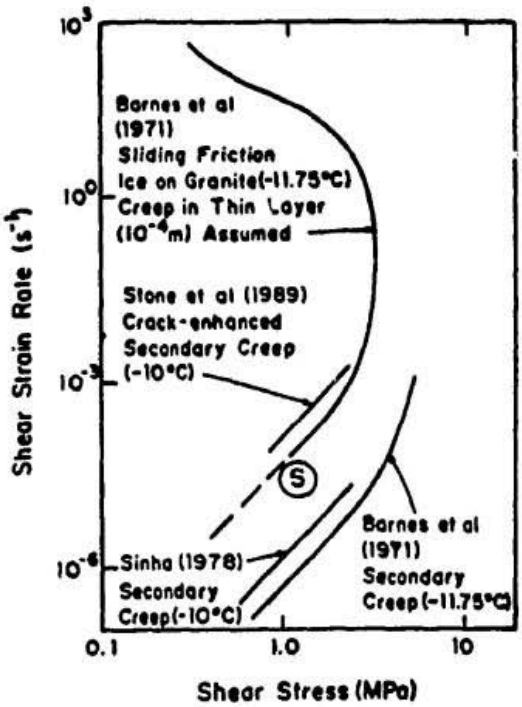


Figure 3.15: Creep and Friction (Jordaan and Mckenna, 1991)

faces and help to soften the layer. The adhesion therefore vanishes. Then the water acting as lubricant makes the coefficient of friction decrease further. The sudden reduction of friction coefficient between cracks make the cracks join together and end up with a fast relative movement of ice particles. The water generated by pressure melting will also reduce the viscosity of the parent ice.

A stick-slip model is presented to account for the whole cycle of dynamic interaction between the ice and indentor (Figure 3.16). The damage enhanced creep theory presented in Chapter 2 contributes to the 'stick' part of the model describing ice deformation at slow strain rates and under low pressure where pressure melting is not important. The 'slip' part of the model is completed by adding a creep enhancement factor $G(p)$ due to pressure melting:

$$\dot{e}_{ij}^{d\prime} = \dot{e}_{ij}^{d} exp(\beta_d S_\sigma) G^d(p) \tag{3.13}$$

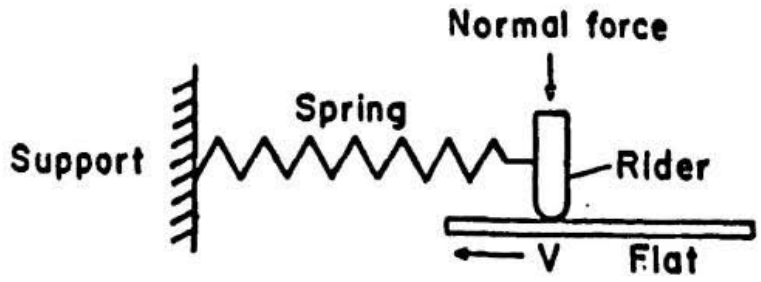


Figure 3.16: Stick-slip Model

$$\dot{e}^{c'}_{ij} = \dot{e}^{c}_{ij} exp(\beta_c S_\sigma) G^c(p), \tag{3.14}$$

where $G(p)$ is the pressure enhancement factor which is a function of hydrostatic pressure $p$. $G(p)$ has the similar softening effect to creep strain as $exp(\beta S_\sigma)$ does.

A number of functions G(p) were tried. The following forms were chosen because they give the best fits to the test results.

$$G(p) = exp(\alpha M),$$

where

$$\frac{dM}{dt} = G_0(\frac{p}{p_0})^g$$

and $p$ is the volumetric stress. In these equations, $\alpha$, $g$, $p_0$ and $G_0$ are constants. Values are chosen by trial and error so as to give a good fit to the field data of indentation tests. Figure 3.17 shows the pressure softening parameter M as a function of volumetric stress. From this figure, one can see that before the pressure builds up, when volumetric stress is small, for example, when the stress is less

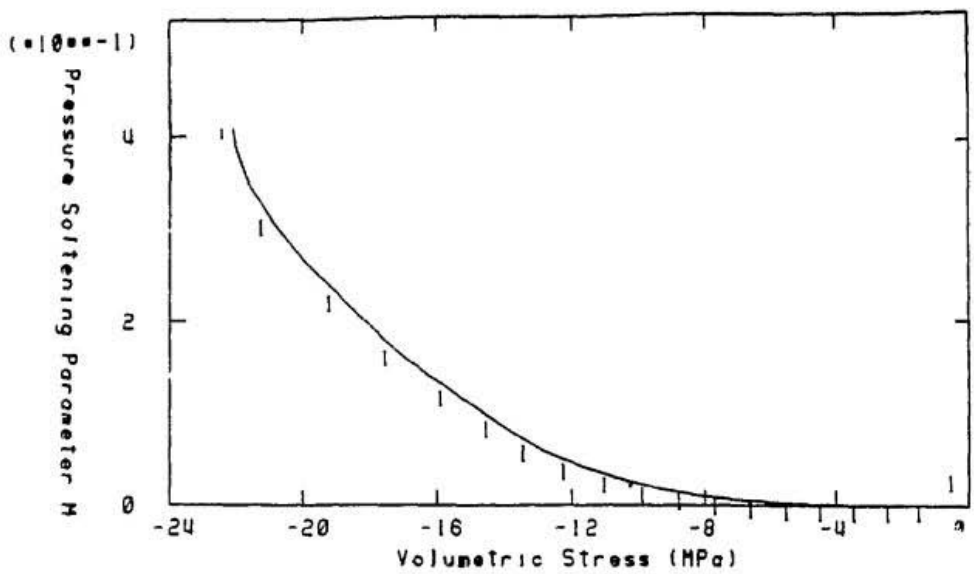


Figure 3.17: Pressure Softening Parameter vs Volumetric Stress

than 10 MPa, the pressure softening parameter is almost zero and $G_p$ is 1. In other words, when the confining pressure is low, the pressure softening effect can be neglected. With the fast increase of volumetric stress, the pressure softening parameter increases quickly.

## 3.3 Summary

Generally speaking, there may be a competition of several mechanisms throughout the ice deformation process in an indentation test. One of them might dominate at a particular stage, for instance, pressure melting may be the main reason for load drop.

Briefly, the hydrostatic stress has the following effects on ice deformation under a triaxial compressive stress:

1. The critical stress and strain for crack nucleation increase with confining

pressure.

2. The early development of multiple axial splitting and shear fracture at high strain rate are suppressed by increasing confining pressure, which turns the brittle failure to a visco-elastic flow enhanced by cracking.

3. Partial or overall closure of microcracks caused by hydrostatic pressure induces traction or frictional sliding between crack surfaces, leading to an increase in stiffness for ice which is already damaged.

4. Once the confining pressure exceeds a certain level, the peak stress decreases with further increase of confining pressure due to the increasing amount of liquid at crack interfaces generated by pressure melting and the softening effects caused by dynamic recrystallization.

5. Pressure melting reduces the coefficient of friction at crack interfaces and the ice viscosity, resulting in a fast deformation of ice.

6. The release of confinement during the load drop will play an important role in ice deformation and must be studied further.

# Chapter 4

# Review of Field Tests

To ensure the stability and the economy of a structural design, an accurate estimation of the ice loads which will be exerted on the structure is essential. Ice-structure interaction is complex and depends on many factors such as the mechanical properties of ice and the structural compliance. It has been found that both medium and laboratory scale ice-structure interaction tests are very helpful in understanding ice forces and in the development of theoretical ice models. Medium scale indentation tests at Hobson's Choice Ice Island, tests of crushed ice between two plates and uniaxial tests of multiyear field ice are discussed in this chapter. One of the indentation tests at Hobson's Choice Ice Island is simulated numerically in Chapter 5. The simulation of the failure process and mechanisms of the ice in front of the indentor are based on the results of the tests of crushed ice between two plates. Material parameters obtained from the uniaxial tests are used in this simulation.

## 4.1 Medium Scale Tests

Medium scale indentation tests have been carried out in the field at Pond Inlet in 1984, at Rae Point in 1985 and at Hobson's Choice Ice Island in 1989 and

1990. A detailed investigation and description of the phenomenon observed in the tests at Hobson's Choice Ice Island have been done by Frederking, Jordaan and McCallum in 1990, Meaney, Kenny and Sinha in 1991, and by Masterson, Frederking, Jordaan and Spencer in 1993. These medium scale indentation tests present a good opportunity to study the characteristics of the failure process and dynamic response, and will be discussed here.

### 4.1.1 Program and Site Description

In May 1990, a field test program was conducted on Hobson's Choice Ice Island Research Station by Memorial University, the National Research Council of Canada (NRC), Canadian Coast Guard (CCG) and Sandwell Swan Wooster (SSW). The test program was fully funded by the Canadian Government through the Canadian Coast Guard Northern and the Panel on Energy Research and Development, and by Amoco Canada Limited, Esso Resources Canada Limited, Conoco Inc., and Mobil Research and Development. The contact pressures for areas up to 1.5 square meters and at indentor speeds of 100 $mm/s$ to 400 $mm/s$ were measured in the tests. The tests were designed to collect data which would help in determining more realistic design ice loads for arctic structures and vessels. Scale effects, ice induced vibrations, and variations in local and global pressures were addressed in this program. The test matrix was a comprehensive plan employing various indentation geometries, contact areas, and structural compliance. There were five test series in this program, these being the TFF series, the TW1 series, the TW3 series, the TFR series, and the SFF series.

Hobson's Choice Ice Island weights approximately billion tonnes and has an

area in plane of 5 km × 8 km. It has a large central portion of freshwater shelf ice surrounded by multiyear sea ice. The tests were conducted predominantly in the multiyear sea ice. The ice structure consists of frazil and columnar-grained ice. Grain size varied from fine to extra-large with some columnar grains up to 50 mm in length. Density ranged from 860 $kg/m^3$ to 890 $kg/m^3$ and the average salinity was about 0.2%. A 100 $m$ long, 3 $m$ deep and 3 $m$ wide trench was excavated and the ice faces were prepared by using a circular saw mounted on a rolling guide. Five indentors were used in the field program: a large flat flexible indentor, a small flat flexible indentor, two wedge indentors with similar construction and a flat rigid indentor. For flat indentors, wedge and pyramidal ice faces were used. The ice surface for the wedge shaped indentor was milled flat. The initial contact widths of the wedge surfaces were 100 mm and 300 mm for the TFF series, SFF series and Test 1 of TFR series. The slope for each side of the wedge was 3:1. The initial contact areas for the pyramid test surface were 100 mm × 100 mm and 500 mm × 500 mm for 4 of the tests in the TFR series.

### 4.1.2 Test Equipment

The area for the large flat flexible and flat rigid indentor was 1.8 $m^2$ (1.2 m × 1.5 m). The area for the small flat flexible indentor was 0.7 $m^2$. A series of hydraulic actuators were used. This configuration was altered to suit the different requirements for each test. A triple actuator system and a single actuator system were used in this program. Up to 4 MN thrust could be given by the single actuator assembly at servo-controlled speed up to 300 $mm/s$. The triple actuator assembly could give up to 12 MN of thrust at a servo-controlled speed of 100 $mm/s$, with

each actuator providing up to 4 MN. An array of sensors were used. The installed sensors included strain gauges, local pressure cells, actuator pressure transducers, a multi-element pressure panel, and an ice surface temperature thermocouple. In one of the indentors, there was a video camera which recorded the interaction process through a window on the indentor. Load cells in the hydraulic actuators and pressure transducers on the face of the indenter gave force-time histories. The ice surface temperature thermocouple gave the variation of the temperature at ice-indentor interface. The arrangement of test equipment in the trench is shown in Figure 4.1.

### 4.1.3 Test Results and Discussion

A detailed understanding of the failure zone near the ice-structure interface is very important to the development of new models of ice-structure interactions. There are basically three regions in the failure zone (Meaney et al., 1991): spall areas ($Z_1$), pulverized areas ($Z_2$) and critical zone or hot spots ($Z_3$). The pressure in the spall areas is very small and can be neglected. Compared with the pressure in critical zone, the pressure in pulverized area is also very small.

The density of the pulverized ice varied from 749 to 846 $kg/m^3$. The parent ice density ranged between 858 to 890 $kg/m^3$. A general trend observed in the tests is that the ice material at the periphery of the contact face appears to be less consolidated than the ice material at the center where the den..ity is almost the same as the parent ice. Investigation of the density distribution suggests that significant dilatation occurs in pulverized areas due to the damage process and low degree of confinement. Large ice particles surrounded by finely pulverized ice

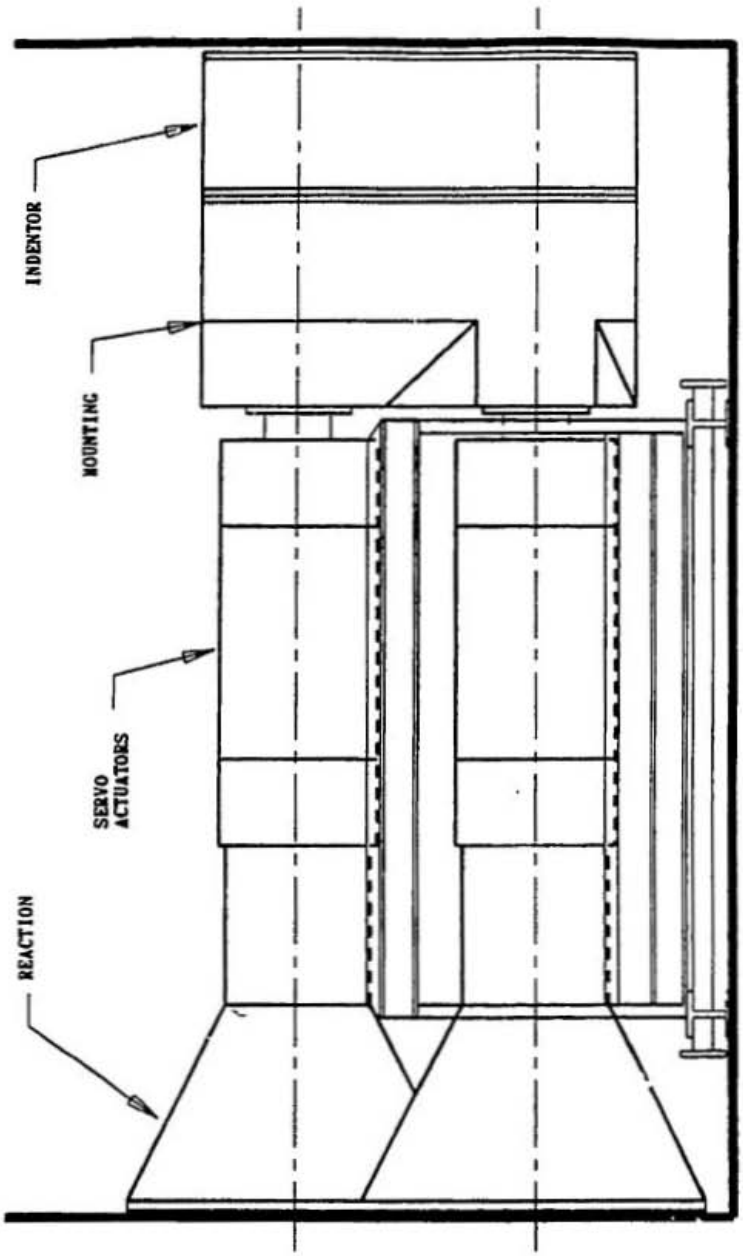


Figure 4.1: Test Equipment in a Trench

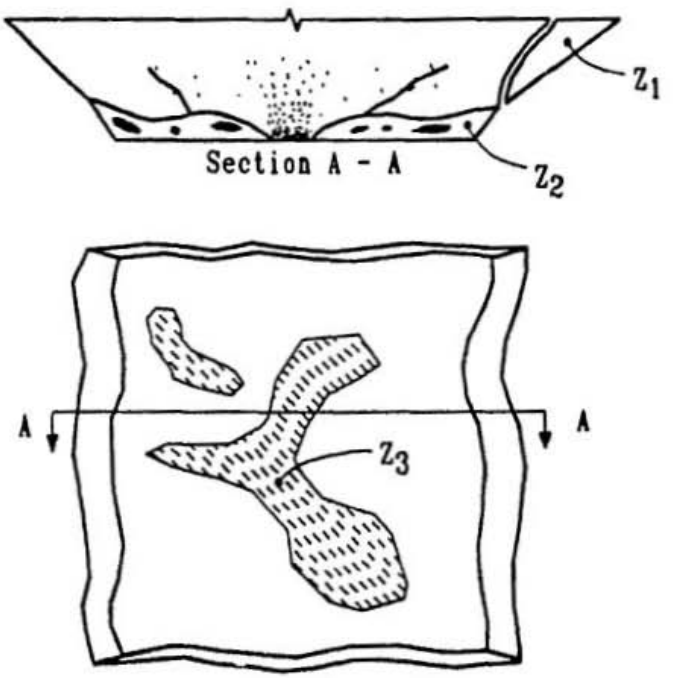


Figure 4.2: Three Regions of Failure Zone (Meaney et al., 1991)

particles are found in pulverized areas, suggesting a grinding action during the extrusion.

After the tests, pulverized ice particles were collected and examined. In the microscopic examination, all particles showed a smooth surface, and had a wetted appearance. No rough or sharp corners were found as would be found if melting did not occur. The large particles in the pulverized areas are found to be a conglomerate of smaller fine particles sintered together. During the tests, very high local pressures and very large pressure gradients had been found across the indentor face. All the evidence given strongly supports the possibility of pressure melting and sintering as an active phenomenon.

The development of the critical zone is affected by many factors. Critical zones usually develop at the center of the interface; this can be identified by the fact that in most cases, the thickness of pulverized layer tends to be largest at the edges and almost zero at the center. In the microscopic investigation, a significant degree of damage and a finer grain structure were found in critical zones than in parent ice. The degree of damage decreased with the distance away from the interface. At a given distance away from the interface, a low degree of damage was found in regions behind the pulverized areas and a high degree of damage was found in regions behind the critical zones. The load history analysis indicated that the local peak pressures varied dynamically in time and location. The features of the failure zones tend to suggest that the peak pressure is related to the critical zones, which carry the majority of the load. Photographs of the test surfaces suggest that the area of the critical zone is approximately 35% of the nominal contact area and ranges from 22% to 55%. All the evidence suggests fundamentally different

deformational processes and mechanisms for the different areas.

## 4.2 Tests of Crushed Ice Squeezed Between Two Plates

The tests of crushed ice squeezed between two plates (Singh et al, 1993) give more information on failure process and the development of the critical zone.

A schematic diagram of the test geometry is shown in Figure 4.3. There is a 100 mm thick layer of crushed ice between two rigid parallel plates. This layer is loaded at a number of constant velocities in y-direction. With the confinement in z direction, the crushed ice is squeezed out along x-direction. The density of the crushed ice is 0.55 $g/m^3$ and the temperature is $-10^oC$. A typical test result of mean pressure and the platen displacement is presented by Singh et al (1992) in Figure 4.4. The process of crushing and extrusion is cyclic. The dynamic behaviour observed in this crushed ice test is similar to that of the medium scale indentation tests. The pressure distribution changes throughout the process but the pressure at the center is always the largest and the pressure near the exit is always the smallest.

In these tests, a high pressure fused zone developed through the compaction of the crushed ice at the center of the platen, and carried most of the load. When the pressure concentrated on the critical zone became high enough, failure started at the edge of the critical zone and then moved towards the center. This caused a sudden pressure increase at the center. The high-pressure gradient forced the ice outwards towards the low pressure zone.

During the loading, ice in the critical zone experiences a cycle of solidification

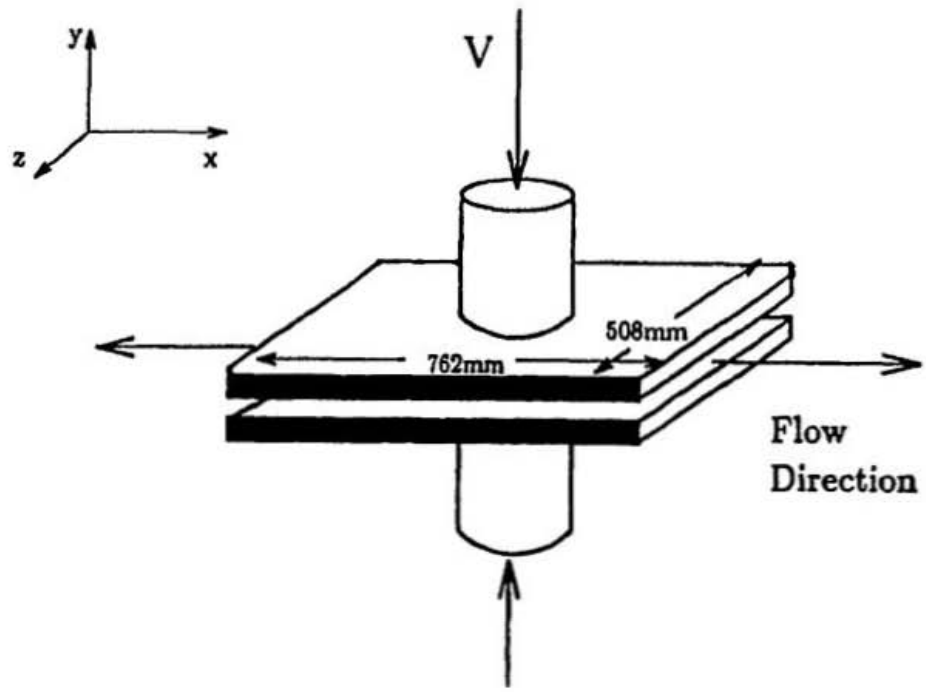


Figure 4.3: Geometry of Crushed Ice Squeezed Between Plates (Singh et al., 1992)

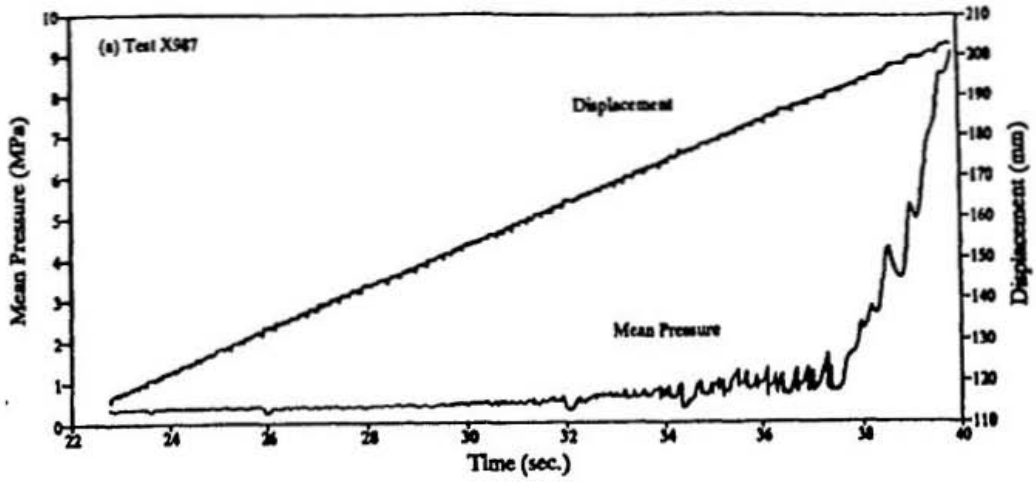


Figure 4.4: Mean Pressure and Platen Displacement (Singh et al., 1992)

sudden pressure increase at the center. The high-pressure gradient forced the ice outwards towards the low pressure zone.

During the loading, ice in the critical zone experiences a cycle of solidification and breaking. The large pressure and confinement which develop in this stage cause the pore structure to collapse and the crystal structure to degrade. A fine grained material therefore begins to form in the critical zone. As the degree of confinement increases, the shear strength decreases. Large contact pressure at the grain boundaries would lead to pressure melting. The melted ice grains sinter as the load drops, reducing the localized shearing. The deformation then is not only caused by grain boundary sliding but also by grain deformation itself. At this moment, the extrusion is solid and very slow resulting in a large load which in turn makes further breaking, melting and sintering possible. According to Singh et al. (1992), the critical zone is described as a fused mass of ice which is believed to

there, enhancing the damage in that region.

## 4.3 Uniaxial Tests

Several cores of multiyear field ice and highly damaged ice from the crushed layer were collected from Hobson's Choice Ice Island during the tests of 1990 and were transported to Memorial University of Newfoundland for uniaxial compressive testing in its laboratory. The purpose of these tests was to investigate the deformation properties of multiyear ice and to obtain the relevant parameters for theoretical modelling. The damage effects were also studied through the tests. Detailed description of the test set up and results were given by Jing Xiao (1991) in his master's thesis.

Comparing the behaviour of the intact ice to the crushed ice, the crushed ice (damaged ice) is much softer. At a strain rate of $5 \times 10^{-4}$, the peak stress of the crushed ice is only 3.49 $MPa$, only 53% of that for the intact ice.

The properties of mutiyear ice were also studied by comparing them to that of freshwater ice (Xiao, 1991). The peak stress of multiyear ice is much lower than that of freshwater ice. Further investigation shows that the elastic behaviour of multiyear ice and freshwater ice are almost the same. If the ice is treated as a Burgers model (Maxwell and Kelvin units), the reason that the multiyear ice is softer must be that it has a lower viscosity (Section 2.13). The lower viscosity may be due to the defects, such as the air pockets in multiyear ice and due to its different crystal structure. For freshwater ice, more than half of the total deformation is elastic, but for multiyear ice, the delayed elastic and secondary creep are the largest components of the total deformation. Both creeps are enhanced by the defects.

The parameters for the finite element model developed by Xiao et al. (1991), are all calibrated from these uniaxial test results and these parameters are used in the present study. The parameters are as following:

| Description | Parameter | Value |
|---|---|---|
| Shear Modulus | G | 3077 MPa |
| Bulk Modulus | K | 6667 MPa |
| Primary Creep Ref. Rate | $\dot{\epsilon}_0^d$ | $8.8 * 10^{-6} s^{-1}$ |
| Secondary Creep Ref. Rate | $\dot{\epsilon}_0^c$ | $1.76 * 10^{-7} s^{-1}$ |
| Creep Exponent | n | 3 |
| Poisson's Ratio | $\nu$ | 0.3 |
| Reference Stress | $\sigma_0$ | 1 MPa |
| Damage Exponent | m | 3 |
| Creep Enhancement Para.1 | $\beta_d$ | 8 |
| Creep Enhancement Para.2 | $\beta_c$ | 18 |

# Chapter 5

# Theoretical Modelling of Indentation Tests

In this chapter, the finite element modelling of one of the indentation tests of the TFR4 series conducted at Hobson's Choice Ice Island in 1990 is described. The indentor used in this test is flat and rigid and moves towards the ice at a constant speed of $100mm/s$ in the whole indentation process. The mass of the indentation system is 9000 $kg$ and the stiffness is 7000 $MN/m$. The ice in contact with the indentor is of pyramidal shape with an initial contact area of $100mm \times 100mm$ and a slope of 1 : 3. The load-time curve of the field test results shows that the total load that the ice exerts on the the indentor increases with time and is characterized by dynamic vibrations. Near the end of the test, in a short period of time, there is a relatively stable condition of dynamic vibration of the load. Figure 5.1 and 5.2 show the load-time and displacement-time curves recorded in this period (Masterson et al., 1993). In 5 cycles of dynamic vibration, the peak loads and minimum loads are almost constant. Approximately, the peak and minimum load are 9 MN and 5 MN, and the frequency is 20 Hz. One can see from these two figures that the indentor moves very slowly when the load builds up and very fast when the load drops.

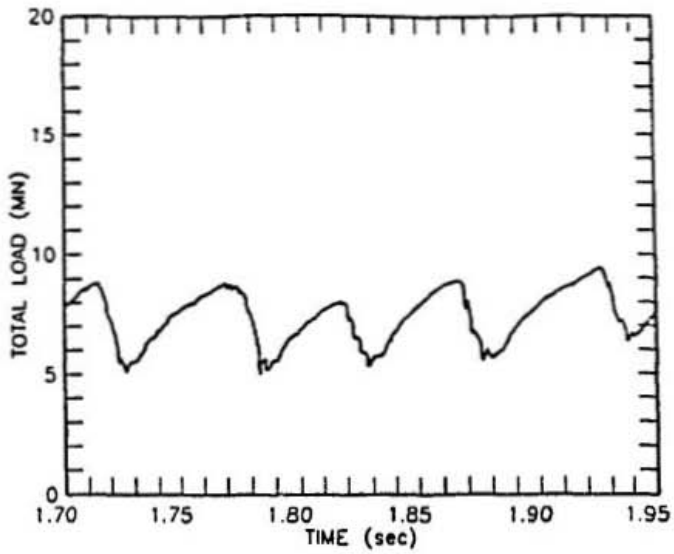


Figure 5.1: Load History of Test Results ( Masterson et al., 1993)

Instead of modelling the whole indentation process from the very beginning, the numerical model simulates only one cycle of interaction when the vibration reaches a relatively stable condition (Figure 5.1 and 5.2). At this moment, the contact area is about $0.8m^2(0.9m \times 0.9m)$. The model results are compared with the field test results. Mechanisms involved in this interaction are also studied.

## 5.1 Model Description

The whole interaction system studied can be divided into two parts: the indentation equipment and the ice.

The model for the indentation equipment consists of a mass, a spring and a dashpot as shown in Figure 5.3. The spring and dashpot elements are placed between the mass element and the fixed end. Only the translational degree of freedom of the indentation system is considered.

The whole ice mesh, including the crushed areas, critical zone, and intact ice,

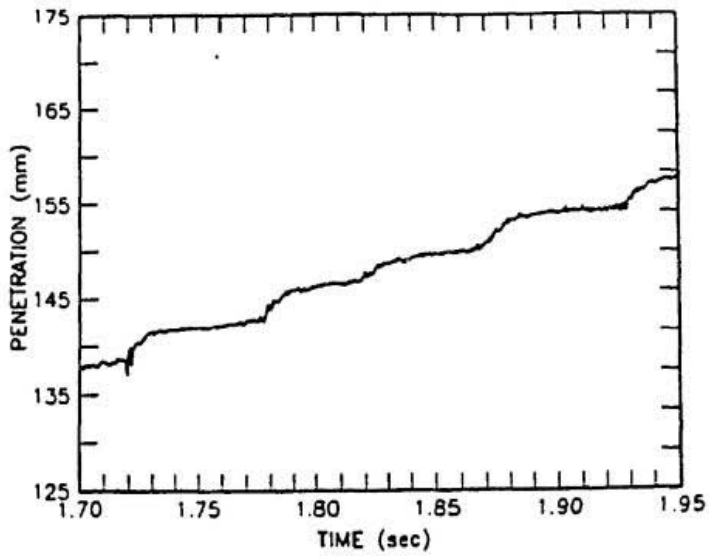


Figure 5.2: Displacement History of Test Results (Masterson et al., 1993)

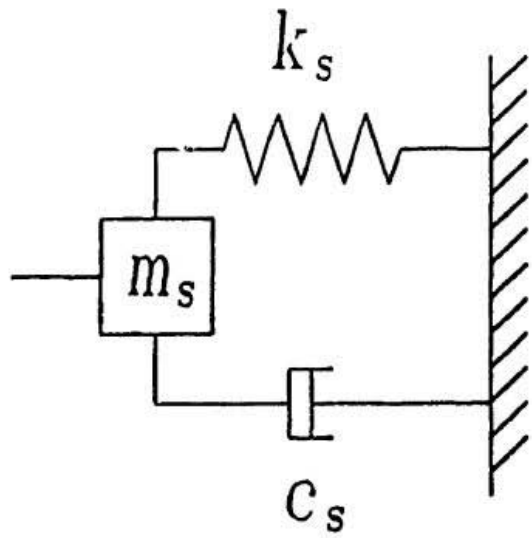


Figure 5.3: Model for Indentation System

shown in Figure 5.4. It has a size of $5m \times 5.2m \times 0.9m$ with an initial contact area of $0.9m \times 0.9m$ at the moment that the vibration cycle considered started. A further assumption made for this numerical interaction model is that the critical zone is concentrated at the central contact area. The ice elements adjacent to the indentor consist of a set of critical zone elements at the geometric center of the contact area and at the edges a set of elements with crushed ice. Different material properties such as the initial damage level, the creep parameter and the elastic modulus are assigned to the crushed ice element set, after Xiao and Jordaan (1991). Figure 5.5 shows the pressure distribution along the whole indentor width. The curve in this figure is obtained when the total ice force exerted on the indentor is about to reach its maximum value. The pressure distribution shows that the load carried by the crushed ice is comparatively small. Ignoring the load carried by the highly damaged crushed and spalled ice, the contact area of the model could be reduced to a thin critical zone at the center along the vertical axis. This reduced initial contact area is assumed to carry all the load exerted by the ice and is assumed to be $0.2m \times 0.9m$, based on the critical zone area suggested by Meaney et al (1991). For simplicity, the load carried by the crushed ice layer is ignored in the following calculation and the corresponding element set is cancelled from the mesh. It is believed that at the moment that the cycle starts, i.e., that the load begins to build up, there will a crushed layer next to the indentor (Figure 5.6), after Xiao et al. (1992). This layer has some degree of initial damage, a lower elastic modulus and a higher creep parameter than that of intact ice. A thin horizontal section through the center of the reduced contact face is used in the model which has only one tenth of the reduced contact area. Due to the symmetrical condition, it is only necessary to

model half of the section. The contact area of the model now is therefore further reduced to only $1/20^{th}$ of $0.2m \times 0.9m$. The total force calculated from this model only represents $1/20^{th}$ of the real force. The mesh of the ice model is shown in Figure 5.6. This mesh has a size of $5m \times 2.6m \times 0.09m$. The final reduced contact area of this ice model is shown in Figure 5.7. A plane strain condition is assumed. An eight-node quadratic element is used. In Figure 5.6, the elements along the right and top edges are infinite elements. Symmetrical conditions are assumed for bottom edge nodes. Interface elements have been defined between the intact and crushed ice.

The ice mesh and the indentation system model are connected by a rigid surface and a set of interface elements. The whole interaction model is shown in Figure 5.8. All the meshes are generated by using finite element technique.

## 5.2 Modelling Theory

The numerical model is generalized to simulate the behaviour of ice in a two dimensional region. The visco-elastic constitutive equation is assumed to be valid for describing the basic ice behaviour. Damage, pressure hardening and pressure melting effects are also included in the model.

Ice will undergo two types of deformation upon loading: the instantaneous elastic deformation and the time-dependent viscous deformation including delayed elastic strain and secondary creep. A time dependent finite element formulation is needed. In order to deal with the material non-linearity, the external boundary condition is applied in an incremental fashion. The time period is divided into steps and the increase in the external boundary condition is assumed to occur at

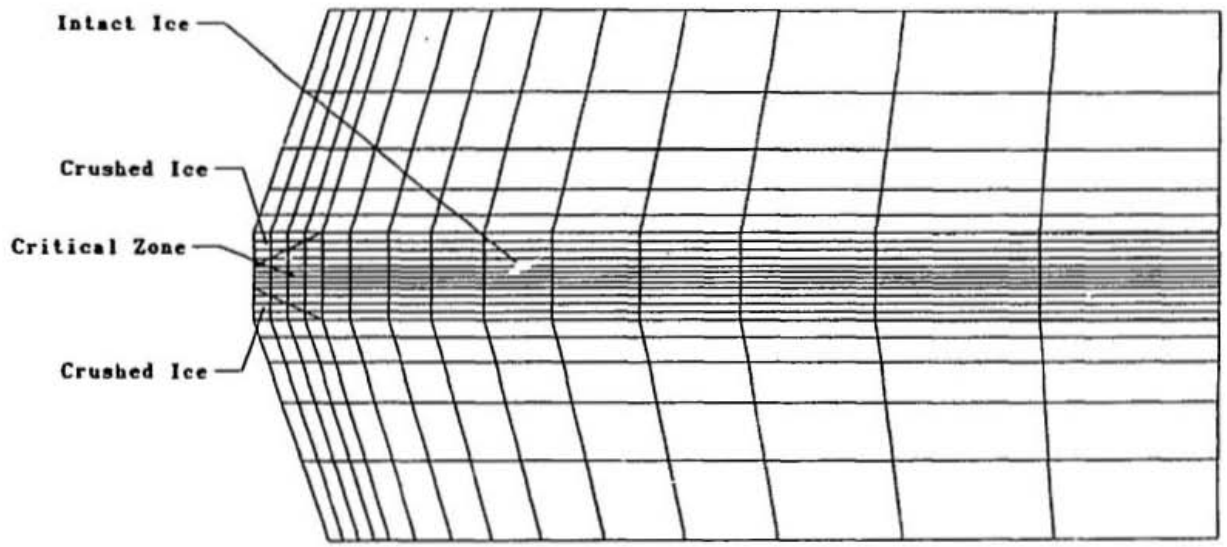


Figure 5.4: The Whole Mesh of Ice Model

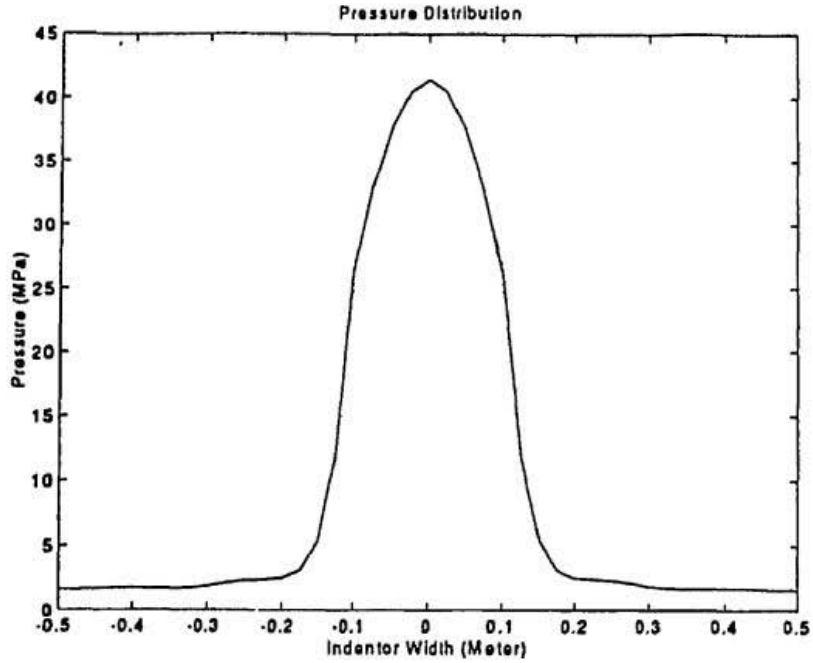


Figure 5.5: Pressure Distribution along Indentor Width

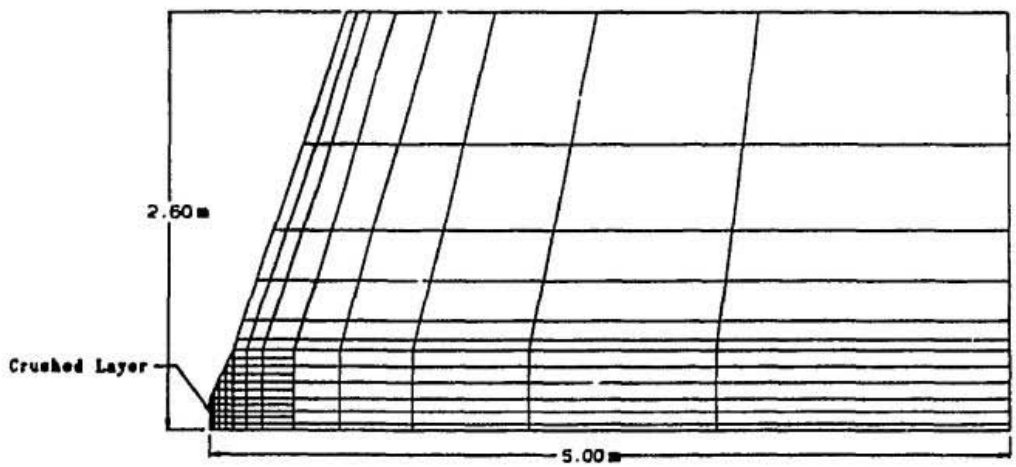


Figure 5.6: The Reduced Ice Mesh

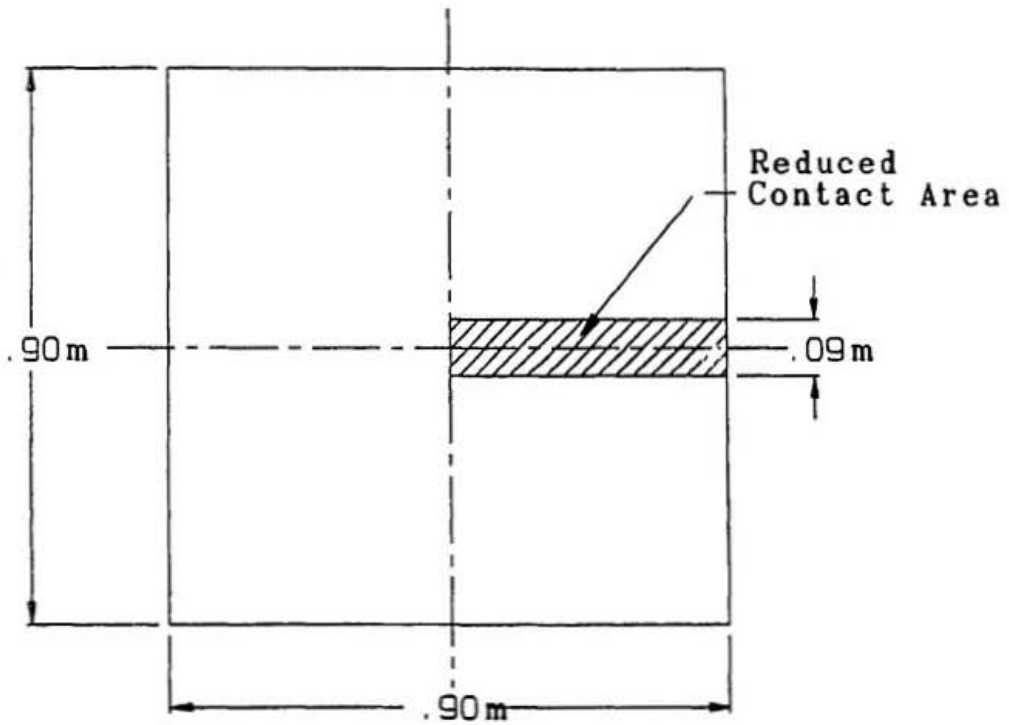


Figure 5.7: The Reduced Contact Area of the Modle

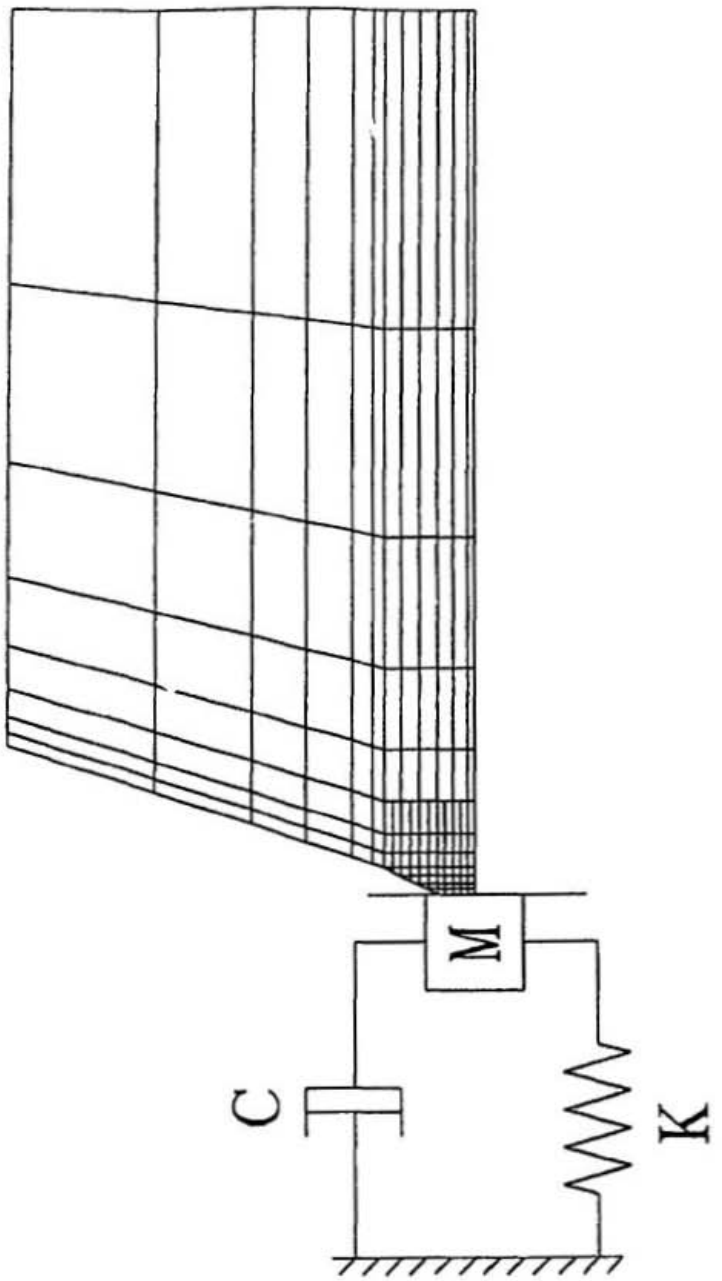


Figure 5.8: Model for Interaction Between Ice and Indentation System

the beginning of the time step so that the external boundary condition is constant within each time step. At the beginning of each increment, the total strain increment is defined in the boundary condition. In a constant speed indentation test, the boundary condition is the indentation speed or strain rate. The total strain increment is:

$$\Delta\epsilon = \frac{\partial\epsilon}{\partial\tau}\Delta t. \tag{5.1}$$

At the beginning of the calculation i.e., the first step, there is no deformation except the elastic strain. The stress is therefore:

$$\sigma_{ij} = K_{ijkl}\epsilon^e_{kl} = K_{ijkl}\epsilon. \tag{5.2}$$

From this stress, the secondary creep rate and the delayed elastic strain rate can be obtained. In the second step, the strains can be obtained from the strain rates.

In the following steps, both the delayed elastic and secondary creep strain can be obtained by using the strain rates obtained in previous step. Therefore, the elastic strain increment is:

$$\delta\epsilon^e_{ij} = \delta\epsilon_{ij} - \delta\epsilon^d_{ij} - \delta\epsilon^c_{ij}. \tag{5.3}$$

The delayed elastic and secondary creep strain rates are therefore obtained in the same way as for the first step (Xiao, 1991):

$$\delta e^d_{ij} = \dot{\epsilon}^d_0\left(\frac{s - 2G_k e^d}{\sigma_0}\right)^n \frac{s_{ij}}{s}\delta t \tag{5.4}$$

and

$$\delta e^c_{ij} = \dot{\epsilon}^c_0\left(\frac{s}{\sigma_0}\right)^n \frac{s_{ij}}{s}\delta t. \tag{5.5}$$

The effect of damage is to reduce the elastic modulus and to enhance the creep strain. The increments of the damage parameter $S_\sigma$, and the bulk and shear moduli are:

$$\delta S_\sigma = S_0(\frac{s}{\sigma_0})^m \delta t \tag{5.6}$$

and

$$\delta K = -K\omega\delta S_\sigma, \tag{5.7}$$

$$\delta G = -G\omega\delta S_\sigma. \tag{5.8}$$

As mentioned in Chapter 2, the delayed elastic and secondary creep strain are enhanced by factors of $exp(\beta_d S_\sigma)$ and $exp(\beta_c S_\sigma)$.

The effect of pressure hardening is accounted for by including the effect of hydrostatic pressure on the damage evolution and the damage rate therefore becomes:

$$\dot{S}_\sigma = S_0(\frac{s}{\sigma_0})^m F(p). \tag{5.9}$$

Pressure melting will soften the material and has the same effects as damage. In addition to the damage enhancement factor $exp(\beta S_\sigma)$, a pressure enhancement factor G(p) is included in the same way as the damage enhancement factor is included in the creep strain equation. A number of the function F(p) and G(p) were tried. The following forms were chosen for use in the example simulation:

$$F(p) = F_0(\frac{p_0}{p})^J \tag{5.10}$$

and

$$G(p) = exp(\alpha M), \tag{5.11}$$

where

$$\frac{dM}{dt} = G_0(\frac{p}{p_0})^g \tag{5.12}$$

and $p$ is the volumetric stress. In these equations, $F_0$, $p_0$, $f$, $g$, $\alpha$ and $G_0$ are constants. Values were chosen so as to give a good fit to the field data from the indentation tests. As well, values were tried for each constant in order to show their influence on the final results.

The stress, strain, damage and pressure effect parameters are all stored as state variables from previous steps; at the end of each increment, they are updated. The model describing the material behaviour has been developed in FORTRAN code and implemented as a user material subroutine in the ABAQUS finite element analysis program.

## 5.3 Modelling Results and Discussion

Since all the parameters used in previous studies about the damaging viscoelastic behaviour of ice were obtained in uniaxial tests, a verification of these parameters in tests with more complex stress condition is recommended. New parameters related to hydrostatic pressure effects have to be calibrated from future triaxial tests too.

The effects of these parameters are demonstrated in Figure 5.9 to Figure 5.12. It is found that the creep parameters $\dot{\epsilon}_0^c$ and $\dot{\epsilon}_0^d$, the damage constant $S_0$, the pressure hardening constant $F_0$, and the pressure softening constant $G_0$ have great effects on the shape and magnitude (peak load) of the load-time curves. The dynamic cycle simulated in the present study starts when the load reaches about $5MPa$; the part of the curve before that point is used for the load building up. The simulation does not start from the beginning but starts from somewhere near the end of the test.

In Figure 5.9 and Figure 5.10, hydrostatic pressure effects are not considered and different values of the creep parameter and the damage constant are tried. The results show that with the decrease of the damage constant, the peak load and the time needed for the peak load to be reached increase while the shape of the load-time curves does not change very much. The creep parameter has a similar effect but the shape of the curves tends to become flatter as the creep parameter increases.

Figure 5.11 shows the results that the pressure hardening effect has on the ice constitutive model. This effect changes the damage distribution significantly. The elements with high volumetric stress have a lower degree of shear damage than those with low volumetric stress; this results in a further stress concentration at the hot spots especially in the central area. The stress in that area will increase with the pressure hardening effects and the ice in the central area of the critical zones will become harder (see the discussion in Chapter 3). The peak ice load obtained from this numerical model increases with the pressure hardening constant $F_0$.

When the pressure softening (melting) effect is included in the ice model, the drop in the total ice force in the load-time curve becomes much sharper; in other words, the shape of the declining side of the curve is much like that of the test result. As can be seen in Figure 5.12, the declining side of the spike of the curve becomes steeper and steeper when pressure softening constant $G_0$ increases. The effect of pressure softening is similar to the effect of damage; both of them enhance the creep deformation significantly. The difference is that the pressure softening is caused by volumetric stress while the damage is caused by shear stress. The pressure softening effect could be viewed as another kind of damage related to hydrostatic

pressure. Thin section analysis shows that in the center of the critical zone, there is a significant degree of damage and the damage mechanism seems quite different from that of shear damage. The peak load decreases with the pressure softening effect (Figure 5.12).

Two typical results of the numerical model which includes both pressure hardening and pressure softening effects are shown in Figures 5.13 and 5.14. In both figures the pressure softening constant is chosen as $G_0 = 12$ and the hardening constant $F_0$ is chosen as 1 and 2. Accurate values of both constants need to be decided in future studies.

Comparing the results obtained by including both pressure hardening and pressure softening effects to the results with only pressure softening effects, it is seen that the peak stress increases when the hardening effect is present. It is also found that the shape of the load history curves when all pressure effects are considered is very similar to those of the test results from the Hobson's Choice Ice Island tests (Figure 5.23). The pressure softening effects soften the ice while the pressure hardening effects make the stress concentrated in the center and the stress gradient becomes much steeper. A steep stress gradient will result in a fast development and progress of shear damage from the edge to the center. A quick extrusion process is therefore expected and so is a sharp drop in total ice force exerted on the indentor. The load and displacement histories obtained by using the suggested model and that of the previous model without considering pressure effects are shown in Figures 5.15 and 5.16. A sharper drop in the ice load and a more accelerated displacement upon load dropping can be seen in the results of t' ggested model.

In Figures 5.17 and 5.18, volumetric stress history and pressure softening pa-

rameter history of 5 elements at the interface in one cycle of interaction are given. In Figure 5.17, curve 1 represents the history of volumetric stress of the element in the geometric center of the ice-indentor contact line while curve 5 represents the edge element and other curves are for intermediate. From the shape and the increase of the volumetric stress in Figure 5.17, a hardening process can be identified in center elements before the ice starts to fail. When the softening or melting effect is accumulated to a certain level, the ice fails. Once the failure starts, the hydrostatic pressure is quickly released. It is seen in Figure 5.18 that the softening effect decreases dramatically from the central element to the edge element and the effect on the edge element (curve 5) is so small that can be neglected.

Figures 5.19 and 5.20 show the variation of pressure distribution during one dynamic cycle. Figure 5.19 is the test result of crushed ice squeezed out between two plates (Singh et al, 1993) and Figure 5.20 is obtained by using the present model. The pressure distribution varies with time in the same way in both results. The presure distribution at different times indicates a build up of pressure in the center and a high pressure gradient across the indentor width due to the hardening effects and the damage development. The high pressure gradient forces the ice outwards towards the low pressure areas, and the pressure softening effect will soften the ice remaining in high pressure zones at the same time.

In Figure 5.21, the two load histories are the results of dynamic and static analysis. Compared to the ice force, the inertial force associated with the vibration of the actuator indentor assembly is very small. In both the dynamic and static analyses, the spring element plays a very important role. In both analyses, there is an acceleration of the mass element after the peak load which simulates the

forward surge of the indentor. Due to the reasons given above, as can be seen in Figure 5.21, there is almost no difference between the two results. Spencer (1993) gave a detailed analysis of the indentation system. He concludes that most of the dynamic response characteristics are a result of the loading and unloading of the model spring. The frequency response of the actuator control system is too low to be able to respond to the rapid displacement changes. It is believed that the load variation is dominated by the deformation of the ice ahead of the indentor, however, the indentation system does have effects on the vibration. When the indentor slows down or surges forward, the servo control system tries to correct and maintain a constant speed. The release of the stored energy in the indentation system after the load peak will also accelerate the vibration.

Xiao et al. (1992) suggest that pressure melting will reduce the friction on both ice-indentor interface and the interface of the damaged ice (crushed layer) and the intact ice. By using this assumption in this numerical modelling, the load history is obtained as shown in Figure 5.22. Further work to prove and include this assumption to the present model is suggested.

Finally, one cycle of the load history results obtained from an example calculation is compared with the corresponding field record from the Hobson's Choice Ice Island tests (Figure 5.23). One can see the good agreement between the model result and the test result.

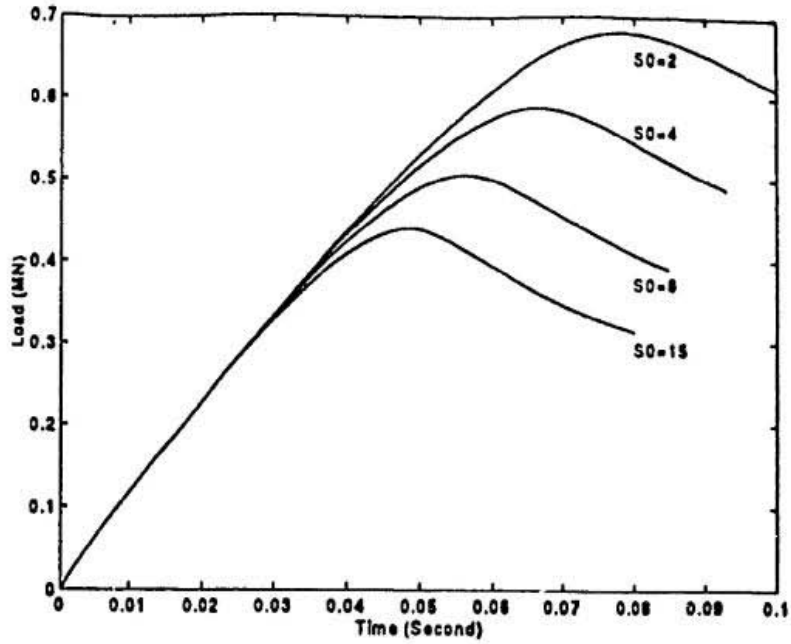


Figure 5.9: Total Ice Force History with Different Damage Constants

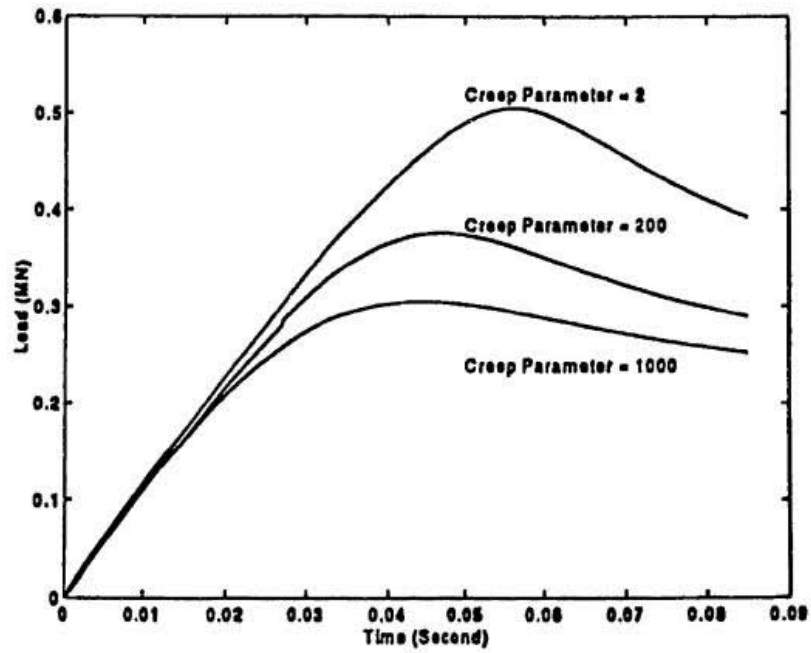


Figure5.10: Total Ice Force History with Different Creep Parameters ($\dot{\epsilon}_0^c$)

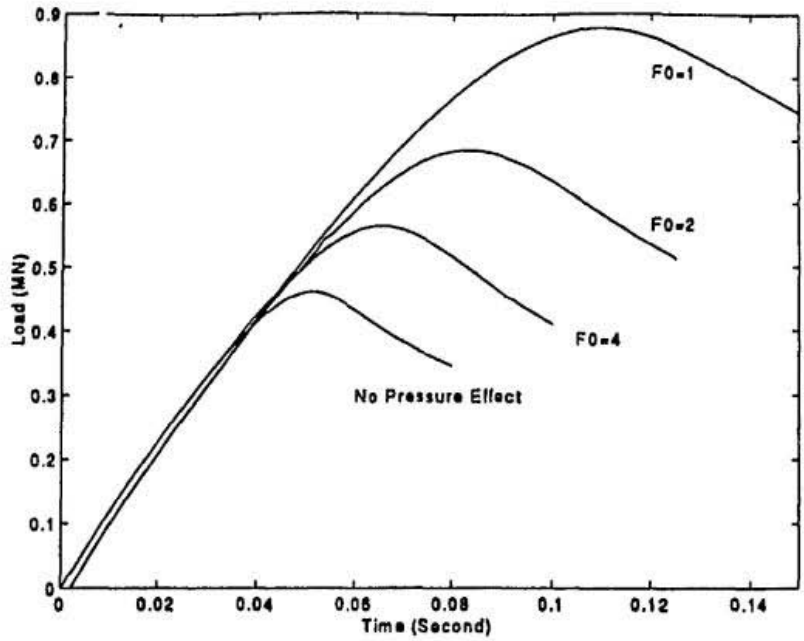


Figure 5.11: Total Ice Force History with Different Pressure Hardening Constant

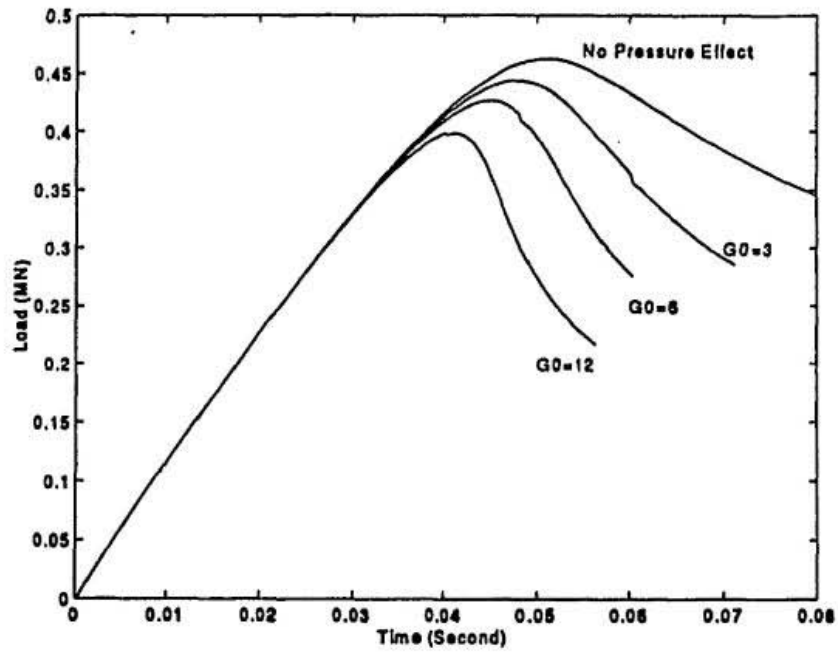


Figure 5.12: Total Ice Force History with Different Pressure Softening Constant

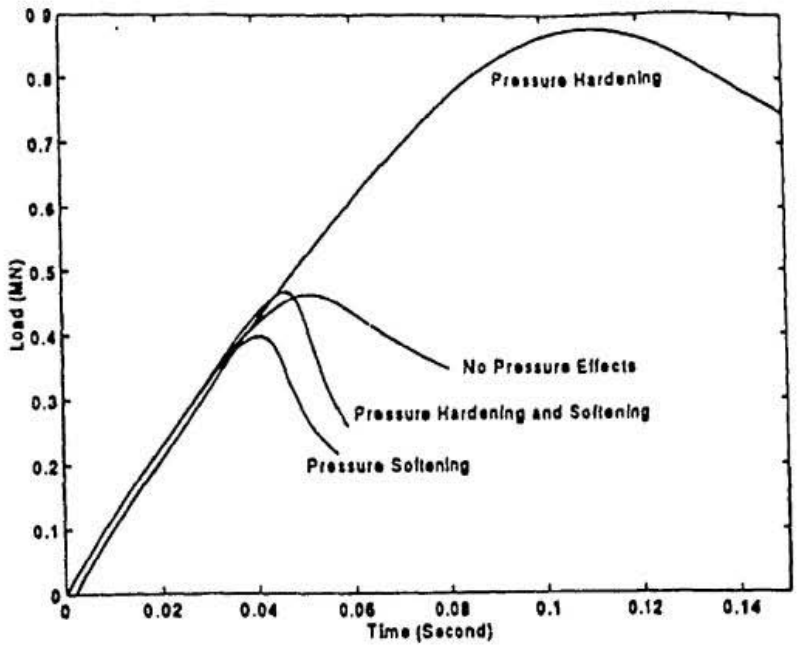


Figure 5.13: Load History With and Without Pressure Effects I, $F_0 = 1$

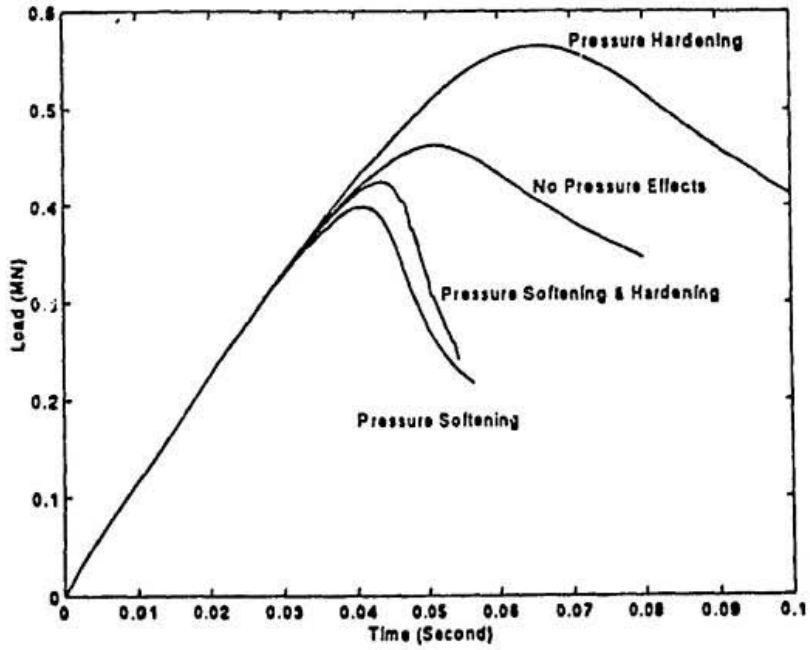


Figure 5.14: Load History With and Without Pressure Effects II, $F_0 = 4$

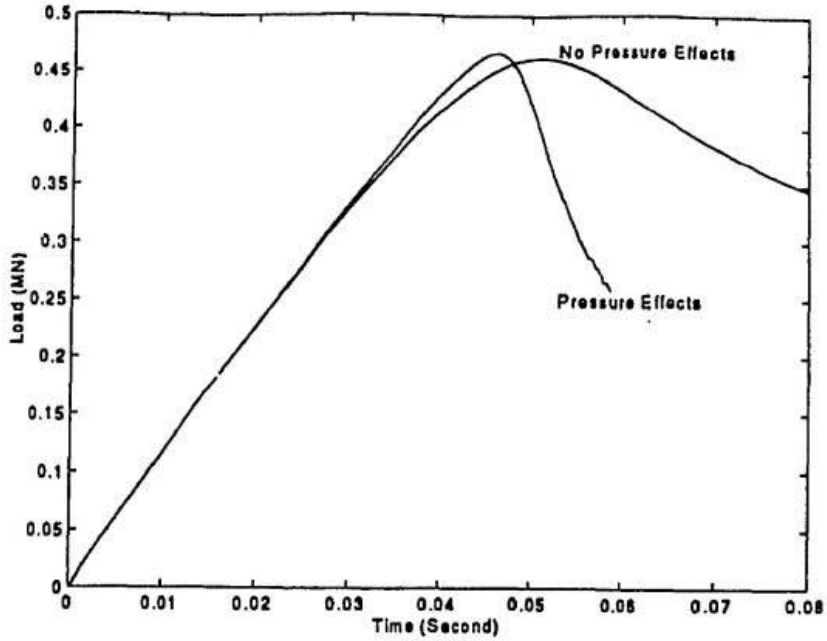


Figure 5.15: Load History of the New Model and the Model without Pressure Effects

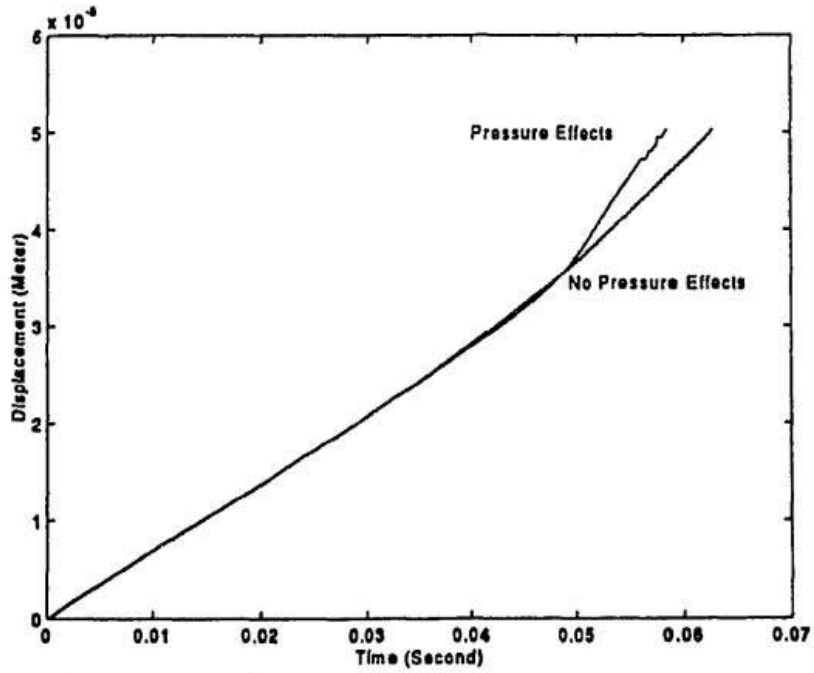


Figure 5.16: Displacement History of the New Model and the Model without Pressure Effects

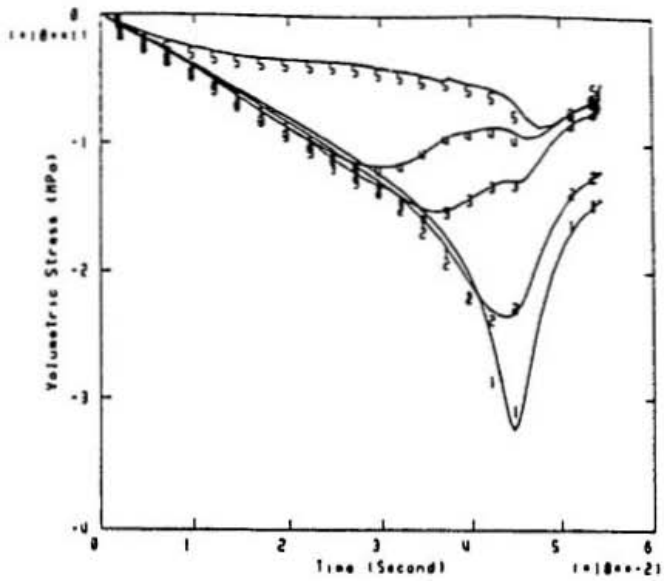

Figure 5.17: Volumetric Stress History

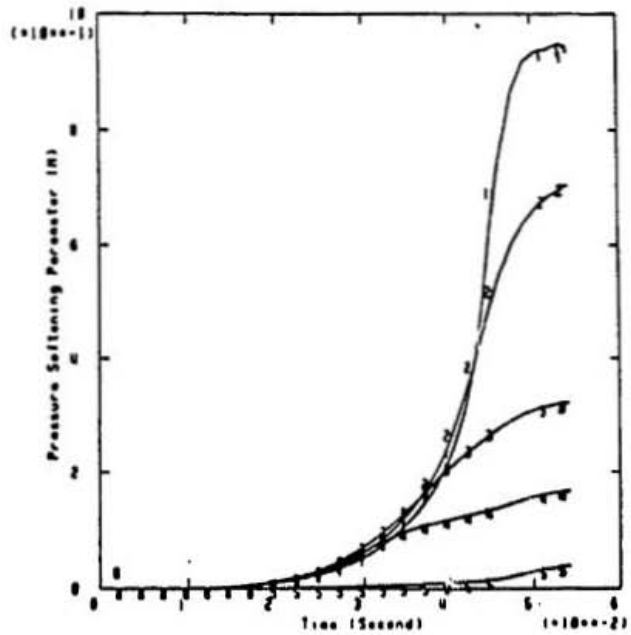

Figure 5.18: The History of Pressure Softening Parameter

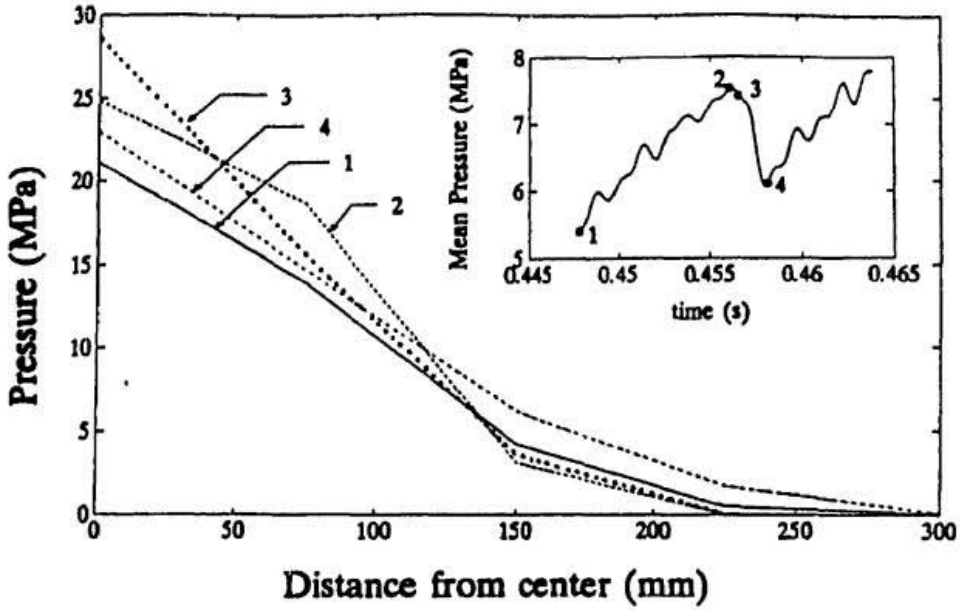


Figure 5.19: Variation in Pressure Distribution of Test Results (Singh et al., 1992)

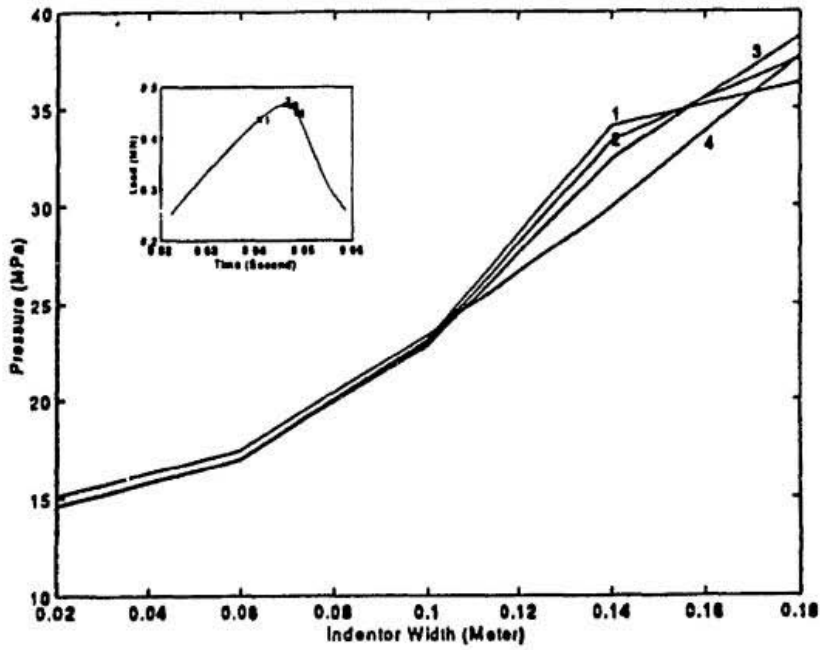


Figure 5.20: Variation in Pressure Distribution of the Modelling Results

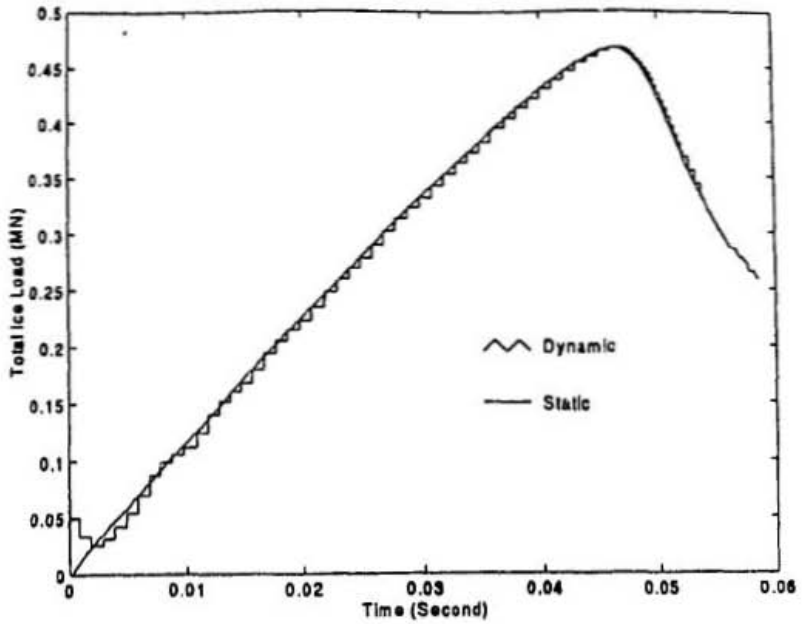


Figure 5.21: Dynamic and Static Modelling Results of Load History

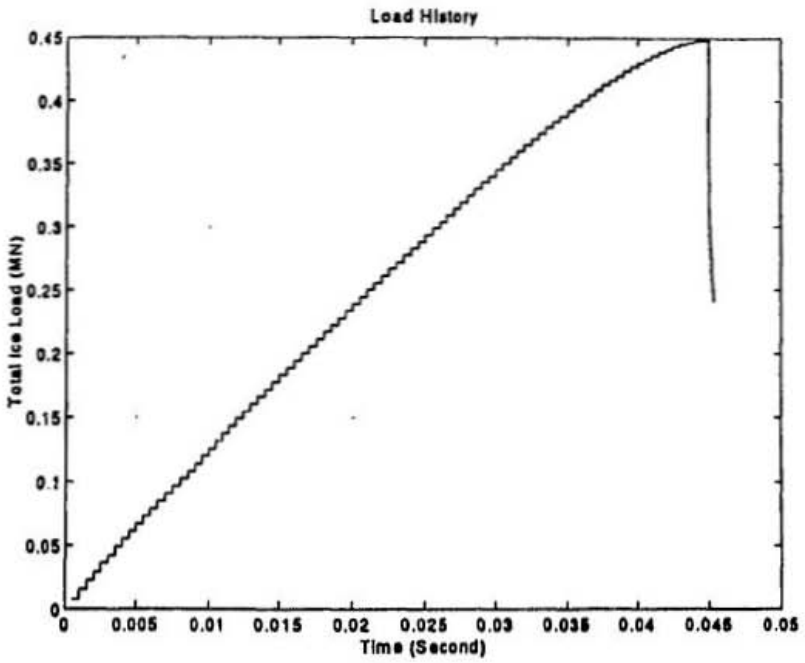


Figure 5.22: Load Vibration Due to the Variation of Friction

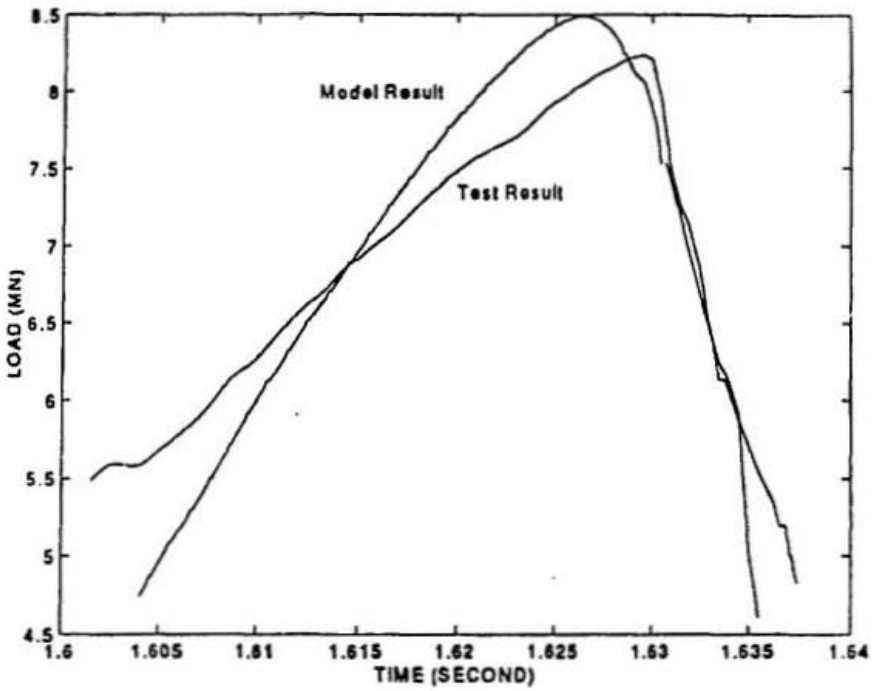


Figure 5.23: Load History of the Model Result and the Test Result

# Chapter 6

# Conclusions and Recommendations

As described in Chapter 3, invaluable information is provided by medium scale indentation tests and small scale laboratory tests. The information regarding the dynamics of the indentation process, distribution of local peak stress and characterization of the failure zone is used in the numerical modelling of the present study.

In a predominantly crushing mode of failure, the ice near the indentor is characterized by the spatial and temporal random distribution of critical zones which are generally associated with regions of moderate to high confinement. Within a critical zone, during fast crushing and clearing indentation events, the development of damage is considered to start from its edges and the damage progression moves rapidly inward. Meanwhile, due to the high confining pressure in critical zones, pressure melting would occur especially in the center area of critical zone where hydrostatic pressure is very high. Pressure melting would further soften ice by reducing its viscosity significantly. It is therefore quite possible to have large deformations in regions of moderate to high confinement.

New models have been proposed by Jordaan (1991) and Schapery (1991) to describe the compressive deformation in ice by using theories of continuum damage mechanics and viscoelasticity. In these models, the loss of deformational resistance is described as ice structure degradation. Previous experimental and numerical results show that the creep strain is significantly enhanced by damage development which is the results of changing structure. The crushed material produced during medium scale indentation tests has varied physical characteristics. Damage mechanisms other than the accumulation of microcracks might be active and hydrostatic pressure would play an important role in such mechanisms. When hydrostatic pressure effects on ice deformation are taken into account in the ice constitutive model in finite element analysis, a very steep pressure gradient is obtained in ice near the indentor which results in both a high level of damage and a quick inward progression of damage. A rapid extrusion of the severely damaged ice is therefore expected. Pressure softening and quick development of microcracking make accelerated creep and extrusion possible. The model of pressure effects on ice in moderate to high hydrostatic pressure condition provides an explanation of the quick failure of ice in indentation tests.

The present study examines the role of damage enhanced creep and hydrostatic pressure effects in ice indentation tests. Pressure melting (softening) and pressure hardening effects are discussed and the suggested models are tried with various functions and parameters. The results are in good agreement with the results from the medium scale indentation tests. Based on the analysis and the numerical calculation results, The following conclusions are made:

1. The development of damage is inhibited by hydrostatic pressure and this will

lead to an increase in stiffness for damaged ice.

2. Once the confining pressure exceeds a certain level, pressure melting can occur and it will reduce the ice viscosity and the friction between crack surfaces, resulting in a fast deformation of the ice in high pressure areas.

3. Damage caused by microcracking and softening effects caused by pressure melting and dynamic recrystallization may be the main reason for load drops in medium scale indentation tests.

4. The development and failure of critical zones can be viewed as the key components in determining the ice load and the dynamic vibration in medium scale indentation tests.

One can see from the numerical modelling results that the shape and the magnitude of the load and displacement are determined by parameters of creep, damage, and pressure effects. To have accurate simulation results, future work should concentrate on identifying these critical parameters which characterize the creep, damage and pressure melting process. Creep enhancement under multiaxial stress states should be a key point in the development of new model. A triaxial test with the release of the confinement when the ice sample fails is suggested in order to simulate the real process during the interaction.

Sintering, which can be viewed as the reverse of the damaging process, may play an important role in helping the load build-up after melting. More detailed study on sintering is necessary for a complete theoretical model of the whole interaction process.

Tensile fracture is not included in the present study although a tensile zone does exist in the ice mesh in finite element analysis. Further study on modelling of fractures and spalls is recommended.

Since the critical zones vary as a function of time and space, probabilistic approaches are suggested.

# References


Ashby, M.F. and Duval, P., 1985. The Creep of Polycrystalline Ice, Cold Regions Science and Technology, Vol. 11, pp. 285-300.

Barnes, P., Tabor, D. and Walker, J.C.F. (1971). The Friction and Creep of Polycrystalline Ice, Proceedings, Royal Society London, A, Volume 324, pp. 127-155.

Bezukhov, N.I., 1953. Theory of Elasticity and Plasticity. Gostekhizdat, Moskva.

Budiansky, B. and O'Connell, R.J. 1976. Elastic Moduli of a Cracked Solid, International Journal of Solids and Structures, Vol.12, pp.81-97.

Cammaert, A.B. and Muggeridge, D.B., 1988. Ice Interaction with Offshore Structures. Van Nostrand Reinhold, New York.

Cannon, N.P., Schulson, E.M., Smith, T.R. and Frost, H.J. (1990). Wing Cracks and Brittle Compressive Fracture, Acta Metallurgica et Materialia, Volume 38, Number 10, pp.1955-1962

Cocks, A.C.F. (1988). A Micromechanics Based Model for the Creep of Ice Including the effects of General Microcracking, Proceedings of the European Mechanics Colloquium 239, Leicester, UK..

Cole, D.M., 1986. Effect of Grain Size on the Internal Fracturing of Polycrystalline Ice, CRREL Report 86-5.

Cole, D.M., 1988. Crack Nucleation in Polycrystalline Ice. Cold Regions Science and Technology, Vol. 15, pp. 79-87.

Cole, D.M., 1989. Microfracture and the Compressive Failure of Polycrystalline Ice. Proceedings IUTAM/IAHR Symposium on Ice-Structure Interaction, St. John's, Newfoundland, Canada, pp. 231-250.

Cormeau, A., Jordaan, I. J., and Maes, M., 1986. Development of a model for progressive damage in ice. Det norske Veritas (Canada) Ltd. Calgary, Alberta.

Currier, J.H. and Schulson, E.M., 1982. The Tensile Strength of Ice as a Function of Grain Size. Acta Metallurgica. Vol. 30, pp. 1511-1514.

Dorris, J.F. 1989. A Plasticity Model for the Crushing of Ice, Proceedings IUTAM/IAHR Symposium on Ice-Structure Interaction, St. John's, Newfoundland, Canada, pp. 311-338.

Finn, D.W., Jordaan, I.J., Singh, S.K. and Spencer, P., 1989. Flow of Crushed Ice: Physical and Mechanical Properties and Behavior, Ocean Engineering Research Centre, Memorial University of Newfoundland, St. John's, NF (proprietary).

Finn, D., 1991. M. Eng. Thesis, Memorial University of Newfoundland.

Flugge, (1967). Viscoelasticity, Blaisdell

Frederking, R.M.W. et al., 1990a. Field Tests on Ice Indentation at Medium Scale, Ice Island, April 1989. National Research Council of Canada Report CR 5866.1.

Frederking, R.M.W., Jordaan, I.J. and McCallum, J.S. 1990b. Field Tests of Ice Indentation at Medium Scale, Hobson's Choice Ice Island, Proc. 10th International IAHR Symposium on Ice, Espoo, Finland, Vol. 2, pp. 931-944.

Gagnon, R.E. and Molgaard, J., 1990. Evidence for Pressure Melting and Heat Generation by Viscous Flow of Liquid in Indentation and Impact Experiments on Ice. Presented at the IGS Symposium on Ice-Ocean Dynamics and Mechanics, Dartmouth College, Hanover, New Hampshire.

Gagnon, R.E. and Molgaard, J., 1990. Crushing Friction Experiments on Freshwater Ice, IUTAM-IAHR Symposium, St. John's, NF., Canada.

Gagnon, R.E. and Sinha,N.K., 1991. Energy Dissipation Through Melting in Large Scale Indentation Experiments on Multi-Year Sea Ice, Proceedings, OMAE, Vol. IV, pp. 157-161.

GEOTECH (GEOTECHnical resources Ltd.), 1985. Medium Scale Iceberg Impact Simulation Test Program, report prepared for Mobil Oil Canada Ltd..

Glen, J.W., 1955. The Creep of Polycrystalline Ice, Proceedings Royal Society of London, Piccadilly, London, W., Ser. A, Vol. 228, pp. 519-538

Gold, L.M., 1970. Process of Failure in Ice. Canadian Geotechnical Journal, Vol. 7, pp. 405-413.

Gold, L.M., 1972. The Failure Process in Columnar-grained Ice, Technical Paper No. 369, Division of Building Research, NRC.

Hallam, S.D., 1986. The Role of Fracture in Limiting Ice Force, Proceedings of IAHR Ice Symposium, Iowa City, Iowa, pp. 287-319.

Hallam, S.D., Duval, P. and Ashby, M.F., 1987. A study of Cracks in Polycrystalline Ice Under Uniaxial Compression, J. de Physique, Tome 48, pp. C1-303-311.

Hausler, F.U., Earle,, E.N. and Gerchow, P. (1988). Uniaxial and Biaxial Compressive Strength of Ice Sampled From Multi-Year Pressure Ridges, Proceedings, Nighth International Conference on Port and Ocean Engineering Under Arctic Conditions, POAC'88, Fairbanks, AK USA., Volume I, pp. 1-12.

Hobbs, P.V. (1974). Ice Physics, Oxford University Press, Bristol, UK.

Horii, H. and Nemat-Nasser, S. 1983. Overall Moduli of Solids with Microcracks: Load-Induced Anisotropy, Journal of Mechanics and Physics of Solids, Vol.31, No.2, pp.155-171.

Horii, H. and Nemat-Nasser, S. 1985. Compression-Induced Microcrack Growth in Brittle Solids: Axial Splitting and Shear Failure, Journal of Geophysical Research, Volume 90, Number B4, pp. 155-171.

Jefferies, M.G. and Wright, W.H. (1988). Dynamic Response of the Molikpaq to Ice-Structure Interaction, Proceedings, Seventh International Conference on Offshore Mechanics and Arctic Engineering, OMAE'88, Houston, TX, U.S.A., Volume 4, pp. 201-220.

Jones, D.E., Kennedy, F.E. and Schulson, E.M. (1991). The Kinetic Friction of Saline Ice Against Itself at Low Sliding Velocities, Annals of Glaciology, Volume 15, pp. 242-246.

Jones, S.J. (1982). The Confined Compressive Strength of Polycrystalline Ice, Journal of Glaciology, Volume 28, Number 98, pp. 171-177

Jordaan, I.J. and Timco, G.W., 1988. Dynamics of the Ice Crushing Process, Journal of Glaciology, Vol. 34, No. 118, pp. 318-326

Jordaan, I.J., Maes, M. and Nadreau, J.P., 1988. The Crushing and Clearing of Ice in Fast Spherical Indentation Tests, OMAE '88, Proceedings of the Seventh International Offshore Mechanics and Arctic Engineering Symposium, Vol. 4, New York, American Society of Mechanical Engineers, pp. 111-116

Jordaan, I.J. and McKenna, R.F., 1988a. Modelling of Progressive Damage in Ice, IAHR Symposium on Ice, Sapporo, Japan, August, Proceedings Vol. II, pp. 585-624

Jordaan, I.J. and McKenna, R.F. 1988b. Constitutive Relations for Creep of Ice, Proceedings International Association for Hydraulic Research (IAHR) Ice Symposium, Sapporo, Japan, Vol.3, pp.47-58.

Jordaan, I.J. and McKenna, R.F. 1989. Processes of Deformation and Fracture of Ice in Compression, Proceedings IUTAM/IAHR Symposium on Ice-Structure Interaction, St. John's, Newfoundland, Canada, pp. 283-310.

Jordaan, I.J., Stone, B.M., McKenna, R.F. and Fuglem, M.K. 1990a. Effect of Microcracking on the Deformation of Ice, Proceedings of the 43rd Canadian Geotechnical Conference, Quebec, pp. 387-393.

Jordaan, I.J., McKenna, R.F., Duthinh, D., Fuglem, M.K, Kennedy, K.P., Maes, M.A. and Marshall, A., 1990b. Development of New Ice Load Models, report for Canada Oil and Gas Lands Administration (COGLA) by (C-CORE), Memorial University, St, John's, NF.

Kachanov, L.M., 1958. On the Creep Rupture Time. Izv. AN SSSR, Ofd. Tekhn. Nauk., No. 8, pp. 26-31.

Kachanov, L.M., 1986. Introduction to Continuum Damage Mechanics. Martinus Nijhoff Publishers.

Kalifa, P., Duval, P. and Ricard, M., 1989. Crack Nucleation in Polycrystalline Ice Under Compressive States, Proceedings, OMAE, A.S.M.E., Vol. 4, pp 13-21.

Karr, D. G., 1985. A damage mechanics model for uniaxial deformation of ice. OMAE'85, Vol. 2, pp. 227-233.

Karr, D.G. and Choi, K., 1989. A Three-Dimensional Constitutive Damage Model for Polycrystalline Ice, Mechanics of Materials, Vol. 8, pp. 55-66.

Katutosi, T. (1977), Friction of a Steel Ball on a Single Crystal of Ice, Journal of Glaciology, Volume 19, Number 81.

Kennedy, K.P., 1990. M. Eng. Thesis, Memorial University of Newfoundland.

Krajcinovic, D., and Fonseka, G. U., 1981. The continuous damage theory of brittle materials, Journal of Applied Mechanics, Vol. 48, pp. 809-824.

Kheisin, D.E. and Cherepanov, N.V. (1970). Change of Ice Structure in the Zone of Impact of a Solid Body Against the Ice Cover Surface, Proceedings, Problemy Arktiki i Antarktiki, Issue 34, pp. 79-84.

Krajcinovic, D., 1983. Constitutive equations for damage materials, Journal of Applied Mechanics, Vol. 50, pp. 355-360.

Kurdyumov, V.A. and Kheisin, D.E. (1976). Hydrodynamic Model of the Impact of a Solid on Ice, Prikladnaya, Volume 12, Number 10, pp 103-109.

Leckie, F.A., 1978. The Constitutive Equations of Continuum Creep Damage Mechanics. Phil. Transactions of the Royal Society, London, Series A, 288, pp. 27-47.

Maattanen, M.P. (1977). Ice Force Measurements at the Gulf of Bothnia by the Instrumented Kemi I Lighthouse, Proceedings, Forth International Conference on Port and Ocean Engineering Under Arctic Conditions, POAC'77, St John's NF, Canada, Volume II, pp. 730-740.

Masterson, D.M., Frederking, R.M.W., Jordaan, I.J. and Spencer, P.A. (1993). Description of Multi-Year Ice Indentation Tests at Hobson's Choice Ice Island - 1990, Proceedings of the 12th International Conference on Offshore Mechanics and Arctic Engineering, OMAE'93, Glasgow, Scotland, UK., Volume IV, pp. 145-155.

McKenna, R.F., Meyssonnier, J. and Jordaan, I.J., 1989. Peak Pressures from a Damage Model for Ice in Compression, Proceedings of the Eighth International Conference on Offshore Mechanics and Arctic Engineering, the Hague, Netherlands, Vol. IV, pp.67-73.

McKenna, R.F., Jordaan, I.J. and Xiao, J., 1990. Analysis of Damage and Energy Flow in the Crushed Layer during Rapid Ice Loading, Proceedings of IAHR Symposium on Ice, Espoo, Finland, Vol. 3, pp. 231-245.

Meaney, R., Kenny, S. and Sinha, N.K. (1991). Medium-Scale Ice-Structure Interaction: Failure Zone Characterization, Proceedings, Eleventh International Conference on Port and Ocean Engineering Under Arctic Conditions, POAC'91, St. John's, NF, Canada, Volume 1, pp. 126-140.

Mellor, M. and Cole, D. M 1982. Deformation and Failure of Ice under Constant Strain-Rate, Cold Regions Science and Technology, Vol. 5, pp. 201-219.

Mellor, M., 1983. Mechanical Behaviour of Sea Ice, U.S. Army Cold Region Research and Engineering Lab,Hanover, CRREL Report 83-1.

Michel, B., 1979. Ice Mechanics, Universite Laval Press.

Molgaard, J. (1990). Mechanisms of Ice Friction, IUTAM-IAHR Symposium, St. John's, NF., Canada.

Murrell, S.A.F, Sammonds, P.R. and Rist, M.A. (1991). Strength and Failure Modes of Pure Ice and Multi-Year Sea Ice Under Triaxial Loading, Proceedings, Symposium on Ice-Structure Interaction, IUTAM/IAHR, St. John's, NF, Canada, pp. 339-361.

Nadreau, J.-P., Mawwar, A.M. and Wang, Y.S. (1988). Triaxial Testing of Freshwater Ice at Low Confining Pressures, Proceedings, Seventh International Conference on Offshore Mechanics and Arctic Engineering, OMAE'88, Houston, TX, U.S.A., Volume IV, pp.117-124.

Nordell, B. (1990). Measurement of P-T Coexistence Curve for Ice-Water Mixture, Cold Regions Science and Technology, Volume 19, pp. 83-88.

Ohno, N., Murakami, S. and Ueno, T., 1985. A Constitutive Model of Creep Describing Creep Recovery and Material Softening Caused by Stress Reversals, Journal of Engineering Materials and Technology, Vol. 107, pp. 1-6.

Pounder, E.R., 1965. The Physics of Ice. Pergamon Press, London.

Resende, L. and Martin, J.B., 1983. Damage Constitutive Model for Geotechnical Applications. Technical report No. 44, Dec. 83.

Resende, L. and Martin, J.B., 1984. A Progressive Damage Continuum Model for Granular Materials. Computer Methods in Applied Mech. and Eng. 42, 1-18 North Holland.

Saeki, H., Ono, T., Nakazawa, N., Sakai, M. and Tanaka, S. (1986). The Coefficient of Friction Between Sea Ice and Various Materials Used in Offshore Structures, Journal of Energy Resources Technology, Volume 19, pp. 65-71.

Sanderson, T.J.O. 1988. Ice Mechanics–Risks to Offshore Structures, Graham and Trotman.

Schapery, R.A., 1981. On Viscoelastic Deformation and Failure Behaviour of Composite Materials with Distributed Flaws. Advances in Aerospace Structures and Materials. The American Society of Mechanical Engineers, pp. 5-20.

Schapery, R. A., 1984. Correspondence Principles and a Generalized J Integral for Large Deformation and Fracture analysis of Viscoelastic Media. Int. Journal of Fracture, Vol. 25, pp. 195-223.

Schapery, R. A., 1991. Models for the Deformation Behaviour of Viscoelastic Media with Distributed Damage and Their Applicability to Ice, Proceedings, Symposium on Ice-Structure Interaction, IUTAM/IAHR, St. John's, NF., Canada, pp. 191-230.

Schapery, R. A., 1988. A theory of mechanical behaviour of elastic media with growing damage and other changes in structure, Mechanics and Materials Center, Texas A and M Univ., College Station, Texas, Report No. MM. 5762-88-1.

Schulson, E.M. and Cannon, N.P., 1984. The Effect of Grain Size on the Compressive Strength of Ice. IAHR Ice Symp. Hamburg. pp. 24-38.

Schulson, E.M., 1987. The Fracture of Ice Ih, J. de Physique, 48: C1-207-220.

Schulson, E.M., 1989. The Tensile and Compressive Fracture of Ice, Proceedings IUTAM/IAHR Symposium on Ice-Structure Interaction, St. John's, Newfoundland, Canada, pp. 165-184.

Schulson, E.M., Hoxie, S.G. and Nixon, W.A., 1989. The Tensile Strength of Cracked Ice. Phil. Mag., Vol. 5 ?, pp. 303-311.

Schulson, E.M. (1990). The Brittle Compressive Fracture of Ice, Acta Metallurgica et Materialia, Volume 38, Number 10, pp. 1963-1976.

Schulson, E.M., Gies, M.C. and Lasonde, G.J. (1989). The Effect of the Specimen-Platen Interface on the Internal Cracking and Brittle Fracture of Ice Under Compression: High-Speed Photography, Journal of Glaciology, Volume 35, Number 121, pp.378-382.

Schulson, E.M. and Smith, T.R. (1992). The Brittle Compressive Failure of Columnar Ice Under Biaxial Loading, IAHR Ice Symposium, Banff, Alberta. pp. 1047-1064.

Schwarz, J., and Weeks,W.,F., 1977. Engineering Properties of Sea Ice, Journal of Glaciology, Vol 19, No. 81, pp 499-531.

Seng-Kiong, T. and Shyam Sunder, S., 1985. Constitutive Modelling of Sea Ice with Applications to Indentation Problems, CSEOE Research Report No. 3, MIT, Cambridge, Massachusetts.

Shyam Sunder, S. and Wu, M.S. 1990. Crack Nucleation due to Elastic Anisotropy in Polycrystalline Ice, Cold Regions Science and Technology.

Singh, S.K., Jordaan, I.J., Xiao, J. and Spencer, P.A. (1993), The Flow Properties of Crushed Ice, Proceedings of the 12th International Conference on Offshore Mechanics and Arctic Engineering, OMAE'93, Glasgow, Scotland, UK., Volume IV, pp. 11-19.

Sinha, N.K., 1978. Rheology of Columnar-Grained Ice, Experimental Mechanics, Vol. 18, No. 12, pp. 464-470.

Sinha, N.K., 1981. Deformation Behaviour of Ice-Like Materials in Engineering Applications, Proc. International Symposium on Mechanical Behaviour of Structured Media, Ottawa, pp. 419-430.

Sinha, N.K., 1982. Delayed Elastic Strain Criterion for First Cracks in Ice, Proc. of the Symposium on Deformation and Failure of Granular Materials, pp. 323-330. Rotterdam: Balkema.

Sinha, N.K., 1983. Creep Model of Ice For Monotonically Increasing Stress, Cold Regions Science and Technology, Amsterdam, Vol. 8, No. 1, pp. 25-33.

Sinha, N.K. 1984. Intercrystalline Cracking, Grain-Boundary Sliding, and Delayed Elasticity at High Temperatures, Journal of Material Science, London, Vol.19, pp. 359-376.

Sinha, N.K., 1988. Crack-Enhanced Creep in Polycrystalline Material: Strain-Rate Sensitive Strength and Deformation of Ice, J. of Materials Science, Vol. 23, No. 12, pp. 4415-4428.

Sinha, N.K., 1989a. Elasticity of Natural Types of Polycrystalline Ice. Cold Regions Science and Technology, Vol. 17, pp. 127-135.

Sinha, N.K. 1989b. Kinetics of Microcracking and Dilatation in Polycrystalline Ice, Proceedings IUTAM/IAHR Symposium on Ice-Structure Interaction, St. John's, Newfoundland, Canada, pp. 69-87.

Sinha, N.K. 1990. In Situ Multiyear Sea Ice Strength and Deformation using NRCC Borehole Indentor. To be presented at OMAE, 1991.

Sjölind, S.G., 1987. A Constitutive Model for Ice as a Damaging Visco-Elastic Material. Cold Regions Science and Technology, No. 41, pp. 247-262.

Sneddon, I.N., 1964. Technical Report AFOSR 64-1989, North Carolina State University.

Spencer, P.A., Masterson, D.M., Lucas, J., and Jordaan, I.J. 1992. The Flow Properties of Crushed Ice I: Experimental Observation and Apparatus, Proc. Symposium on Ice Intl. Association of Hydraulics Research, Volume I. pp. 158-168.

Spencer, P.A., Masterson, D.M. and Metge, M., 1993. The Flow Properties of Crushed Ice: Crushing Plus Extrusion Tests, International Conference on Offshore Mechanicas and Arctic Engineering.

Stone, B.M., Jordaan, I.J., Jones, S.J. and McKenna, R.F. 1989. Damage of Isotropic Polycrystalline Ice Under Moderate Confining Pressures, Proceedings of the 10th International Conference on Port and Ocean Engineering under Arctic Conditions, Lula, Sweden, Vol.1, pp.408-419.

Timco, G.W., 1986. Indentation and Penetration of Edge-Loaded Freshwater Ice Sheets in the Brittle Range, Fifth OMAE Symposium, Proceedings Vol. IV, pp. 444-452

Timco, G.W. and Jordaan, I.J., 1988. Time-Series Variations in Ice Crushing, POAC '87, Proceedings of the 9th International Conference on Port and Ocean Engineering Under Arctic Conditions, Fairbanks, Alaska, pp. 13-20.

Tomin, M., Cheung, M., Jordaan, I.J. and Cormeau, A., 1986. Analysis of Failure Modes and Damage Processes of Freshwater Ice in Indentation Tests. Proc. of 5th OMAE Symp., Tokyo, Vol. IV, pp. 453-460.

Wang, Y.S., 1979a. Sea Ice Properties. Technical Seminar. Exxon Company, USA.

Wang, Y.S., 1979b. Crystallographic Studies and Strength tests of Field Ice in the Alaskan Beaufort Sea. In POAC 79, pp. 651-655.

Wang, Y.S., 1981. Uniaxial Compression Testing of Arctic Sea Ice. Proc. of 6th POAC, Vol. 1, pp. 346-355.

Weeks, W.F. and Assur, A., 1967. The Mechanical Properties of Sea Ice. CRREL Monograph II-C3.

Weertman,J., 1969. Effects of Cracks on Creep Rate, Transactions Quarterly, Transactions of the ASM, Vol. 62, No. 2, pp. 502-511.

Xiao, J. and Jordaan, I.J., 1991. Modelling of Fracture and Production of Discrete Ice Pieces, a report prepared for Canada Oil and Gas Lands Administration (COGLA).

Xiao, J., Jordaan,I.J., McKenna, R.F. and Frederking, R.M.W., 1991. Finite Element Modelling of Spherical Indentation Tests on Ice. Proc. of the 11th International Conference on Port and Ocean Engineering under Arctic Conditions, Sept., 1991, St. John's, NFLD.

Xiao, J. (1991). Finite Element Modelling of Damage Processes in Ice- Structure Interaction, M.Eng. Thesis, Memorial University of Newfoundland, St. John's NF, Canada.

Xiao, J., Jordaan, I.J. and Singh, S.K. (1992). Pressure Melting and Friction in Ice-Structure Interaction, Proceedings, Symposium on Ice, Int. Association of Hydraulics Research, Volume 3.